Pós-Graduação em Ciência da Computação

LEON DENIS DA SILVA

A discrete exterior calculus approach to quantum transport on surfaces

Universidade Federal de Pernambuco
posgraduacao@cin.ufpe.br
http://cin.ufpe.br/~posgraduacao

Recife
2019

LEON DENIS DA SILVA

A discrete exterior calculus approach to quantum transport on surfaces

Thesis presented to the Postgraduate Program in Computer Science from the Universidade Federal de Pernambuco, as a partial requirement for obtaining the title of Doctor of Computer Science.

Concentration area: Media and Interaction.

Advisor: Prof. Dr. Silvio de Barros Melo

Co-advisor: Prof. Dr. Antonio Murilo Santos Macêdo

Recife
2019

Catalogação na fonte
Bibliotecária Mariana de Souza Alves CRB4-2105

S586d Silva, Leon Denis da
A discrete exterior calculus approach to quantum transport on surfaces/ Leon Denis da Silva – 2019.
52 f., fig., tab.

Orientador: Silvio de Barros Melo.
Tese (Doutorado) – Universidade Federal de Pernambuco. CIn, Ciência da Computação. Recife, 2019.
Inclui referências e apêndices.

1. Mídia e Interação. 2. Cálculo exterior discreto. 3. Espalhamento quântico. 4. Funções de Green recursisvas. I. Melo, Silvio de Barros (orientador). II. Título.

006.7 CDD (22. ed.) UFPE-MEI 2019-166

Leon Denis da Silva

"A Discrete Exterior Calculus Approach to Quantum Transport on Surfaces"

Tese de Doutorado apresentada ao Programa de Pós-Graduação em Ciência da Computação da Universidade Federal de Pernambuco, como requisito parcial para a obtenção do título de Doutor em Ciência da Computação.

Aprovado em: 25/10/2019.

_____

Orientador: Prof. Dr. Silvio de Barros Melo

BANCA EXAMINADORA

_____

Prof. Dr. Adenilton José da Silva
Centro de Informática / UFPE

_____

Prof. Dr. Ricardo Martins de Abreu Silva
Centro de Informática / UFPE

_____

Prof. Dr. Stefan Michael Blawid
Centro de Informática / UFPE

_____

Prof. Dr. Anderson Luiz da Rocha e Barbosa
Departamento de Física / UFRPE

_____

Prof. Dr. Francisco Assis Gois de Almeida
Departamento de Física / UFS

my wife, Giselly.

ACKNOWLEDGEMENTS

First of all, I thank my wife Giselly for her presence and patience during all stages of my long path of academic titles (undergraduate, masters, and doctorate).

To my family, for their unconditional support, concern all the crucial moments of my life.

To Dr. Silvio de Barros Melo, advisor, for his availability, welcome, and discussion throughout this work.

To my co-advisor, Dr. Antônio Murilo Santos Macêdo, for his availability, patience, and guidance on the subject of this work.

To my friend Carlos Batista, for the group spirit, companionship, and long conversations on the subject of this work.

To Professor Dr. Wilson Rosa, for his patience, advice, and helpful conversations on all topics of life. Besides, our discussions about math and computing were essential to the completion of this work.

Thanks to the friends from postgraduate studies, with whom I shared enjoyable moments, especially Jamerson, Jerônimo, Rhudney, Edilson, and Maigan.

I thank my friends José Deibsom, Francisco Calvi, Filipe Mendonça, and Tiago Veras, who has been with me for a long time on this journey.

I thank the Department of Mathematics - UFRPE, where I am a professor, for all the support that was needed.

I thank the Heineken brewery; without it, everything would be more difficult.

And finally, to the CIn-UFPE for the beautiful and welcoming research environment.

ABSTRACT

We address the problem of computing transport observables on arbitrary surfaces. Our approach is based on discrete exterior calculus (DEC) and applies to open quantum systems. The curved system is approximated by a simplicial complex consisting of flat triangles where each vertex is located on a smooth surface. Was developed a discretization of Schrödinger equation and the associated Green's functions. Such an approach allowed for the formulation of the tight-binding Hamiltonian based in discrete calculus exterior. We present an efficient algorithm for the calculation of the recursive Green's functions using numerical tools available for DEC. In addition to working with curved surfaces, our discretization shares the advantages of the Finite Differences Method when submitted to mesh in flat space. Our approach is applied to the calculation of the conductance of a non-flat quantum device coupled to electron reservoirs defined on curved surfaces. We found numerical evidence of a curvature induced integrable-chaotic crossover.

Keywords: Discrete exterior calculus. Quantum scattering. Recursive Green's function. Schrödinger.

RESUMO

Abordamos o problema de computar observáveis de transporte em superfícies arbitrárias. Nossa abordagem é baseada em cálculo exterior discreto (DEC) e aplica-se a sistemas quânticos abertos. O sistema curvo é aproximado por um *simplicial complex* que consiste de triângulos planos, onde cada vértice está localizado em uma superfície suave. Foi desenvolvida uma discretização da equação de Schrödinger e das funções de Green associadas. Tal abordagem permitiu a formulação do hamiltoniano, do tipo *tight-binding*, com base no cálculo exterior discreto. Apresentamos um algoritmo eficiente para o cálculo das curvas recursivas de Green. Além de trabalhar com superfícies curvas, nossa discretização compartilha as vantagens do Método de Diferenças Finitas quando submetido a um domínio plano, nossa abordagem é aplicada ao cálculo da condutância de um dispositivo curvo acoplado a reservatórios de elétrons definidos em superfícies curvas. Encontramos evidências numéricas de um cruzamento caótico-integrável induzido por curvatura.

Palavras-chaves: Cálculo exterior discreto. Espalhamento quântico. Funções de Green recursivas. Schrödinger.

LIST OF FIGURES

LIST OF TABLES

LIST OF SYMBOLS

G^r	Retarded Green's function
G^a	Advanced Green's function
$\mathscr{H}$	Hamiltonian
W	Vector space
Ω^k	Space of differential k-forms over W
ω	k-form
$\bar{\omega}$	k-cochain
$\mathscr{K}$	Simplicial mesh
$\star\mathscr{K}$	Dual simplicial mesh
σ^k	Primal k-dim element of $\mathscr{K}$
$\star\sigma^k$	Dual k-dim element of $\star\mathscr{K}$
$\mathscr{C}^k(\mathscr{K})$	space of primal k-cochain
$\mathscr{D}^k(\star\mathscr{K})$	space of dual k-cochain.
d_k	k^{th} discrete exterior derivative operator
$*_k$	k^{th} discrete Hodge star operator
∂_k	k^{th} discrete boundary operator

CONTENTS

1 INTRODUCTION

1.1 THE SCATTERING PROBLEM

Solving the scattering problem is one of the most common and general tasks in condensed matter physics. Instead of describing states in a closed geometry, one considers the scattering of particles in a finite system coupled to infinite leads. Green's functions are known to be a convenient tool to solve linear differential equations, including the Schrödinger equation in quantum mechanics. Finding the scattering matrix, or the Green's function, associated with a quantum scattering, or bound-state, the problem is tantamount to solving the time-independent Schrödinger equation. Depending on the geometry of the scattering region, an analytical approach could become a daunting, if not an impossible, task. A valuable alternative is to employ numerical techniques based on discretization models which could in principle allow direct computation of all relevant observables.

Several discretization methods have been used in quantum calculations, among them the finite difference (FDM) and finite element (FEM) methods. The finite difference method is the standard procedure for transforming a differential equation into a difference equation. It is perhaps the most mature and successful numerical approach in quantum numerical simulations for both two-dimensional (albeit only in flat geometries) and three-dimensional domains (FERRY; GOODNICK, 1997; DATTA, 2005). FDM is used in crucial numerical quantum transport simulation software, such as Nanomos (REN et al., 2003) and Kwant (GROTH et al., 2014). Over the years, the finite element method (FEM) has been used as an alternative to FDM in many applications, such as in calculations of electronic structures of materials (KOJIMA; MITSUNAGA; KYUMA, 1989; TSUCHIDA; TSUKADA, 1995; TSUCHIDA; TSUKADA, 1996; PASK et al., 2001), electromagnetism (ASSOUS et al., 1993; WONG; PICON; HANNA, 1995) and fluid dynamics (TAYLOR; HOOD, 1973; TUANN; OLSON, 1978), to name a few. More recently, stimulated by the simplicity in the treatment of boundary conditions, precision control through mesh refinements and the ability to represent regions with complex geometries, the FEM has been adopted to compute Green's functions in two-dimensional structures to calculate transport properties of quantum devices (HAVU et al., 2004; KURNIAWAN; BAI; LI, 2009).

There are several reasons for the substitution, in real physical problems, of the standard discretization methods of FEM and FDM by others that, in addition to discretizing the geometry, preserve topological structures and the classical theorems of calculus on surfaces (DESBRUN; KANSO; TONG, 2008; GRADY; POLIMENI, 2010; TONTI, 2014; FERRETTI, 2014; ALOTTO FABIO FRESCHI, 2013). In this direction, several works have adopted the discrete exterior calculus (DEC) (HIRANI, 2003; DESBRUN; KANSO; TONG, 2008) for the numerical treatment of problems described by differential equations with several types of boundary conditions (GRADY; POLIMENI, 2010; RUFAT et al., 2014; GOES et al., 2016), with important applications in electro-

magnetism (STERN et al., 2015; RABINA; MONKOLA; ROSSI, 2015; CHEN; CHEW, 2017b) and fluid dynamics (MOHAMED; HIRANI; SAMTANEY, 2016b; NITSCHKE; REUTHER; VOIGT, 2017) in two (including curved domains) and three dimensions. In the various DEC approaches cited above, comparisons showed computational time and precision compatible with typical discretization models (including FDM and FEM) and the expected integration between topology, geometry and the physical quantities involved. In a nutshell, DEC is a method of discretization of differential forms and their operators (Hodge star, exterior derivative, wedge product), which are usually present in the formulation of differential equations on manifolds. Just as FEM, DEC is based on structured and unstructured simplicial meshes. Therefore, it is adaptable to solve scattering problems in arbitrary complex structures. Its main advantage is the alignment between the continuous and the discrete theory making numerical approaches with DEC less susceptible to spurious solutions, see Refs. (DESBRUN; KANSO; TONG, 2008).

The effects of curvature and topology have also been a major subject in condensed matter physics. Several models have been developed to model curvature and to study its influence on the physical properties of materials. Studies on the Schrödinger equation confined to a curved surface showed the presence of a quantum geometry-induced potential expressed in terms of both Gaussian and Mean curvatures (JENSEN; KOPPE, 1971; COSTA, 1981). Years later, ENCINOSA; ETEMADI, used the benefits of differential forms to produced results identical to those of COSTA. Since then, geometric effects has been the subject of intensive research (ENCINOSA; MOTT, 2003; MARCHI et al., 2005; TAIRA; SHIMA, 2007; ATANASOV; DANDOLOFF, 2007; ATANASOV; DANDOLOFF, 2008; SANTOS et al., 2016; SILVA; BASTOS; RIBEIRO, 2017). Shortly after the discovery of graphene, the Dirac Hamiltonian to curved surface (SUZUURA; ANDO, 2002; VOZMEDIANO; JUAN; CORTIJO, 2008) has been applied to investigate the electronic properties of curved graphene sheets (JUAN; CORTIJO; VOZMEDIANO, 2007; CORTIJO; VOZMEDIANO, 2007b; CORTIJO; VOZMEDIANO, 2007a; KERNER; NAUMIS; GÓMEZ-ARIAS, 2012). More recently, STEGMANN; SZPAK, using a tight-binding model and the non-equilibrium Green's function method, presented a study of the effect of curvature on the current flow lines on elastically deformed graphene sheets (STEGMANN; SZPAK, 2016). It is generally understood that a complete understanding of the full potential of graphene must include the effects of curvature in its physical properties.

In the present thesis, we address the problem of including geometric features, such as curvature, in the calculation of transport and spectral characteristics of quantum devices. More specifically, we propose a DEC based numerical algorithm to solve quantum scattering and bound-state problems in confined systems defined on arbitrary curved surfaces. The choice of DEC in this thesis is mainly due to its applicability to simulate physical processes on curved surfaces, unlike the FDM and the FEM approaches. In Chapter 2, we present a brief review of the Green's function formalism, while the DEC discretization is presented in Chapter 3. In Chapter 4, we describe two DEC-based models to compute Green's functions associated with a quantum scattering problem on curved surfaces. The comparison between DEC-based discretization and

the finite difference method in flat surfaces is performed in Section 4.2. We closed the chapter illustrating our DEC approach by calculating the conductance of a curved device. We observed a qualitative change in the conductance as a function of energy, which goes from a smooth dependence for a flat system to an irregular noisy type of behavior as the curvature is increased. Finally, in Chapter 5 we give a summary of our main results and conclusions. In Appendix A, the computational time efficiency of our numerical approach is analyzed.

1.2 LIST OF PUBLICATIONS

This thesis is based on the content of a manuscript. Under the supervision of A. M. S. MACÊDO, W. R. DE OLIVEIRA and S. B. MELO we did:

- **L. D. DA SILVA**, C. A. BATISTA , I. R. R. GONZÁLEZ, A. M. S. MACÊDO, W. R. DE OLIVEIRA, S. B. MELO. A discrete exterior calculus approach to quantum transport and quantum chaos on surfaces. Journal of Computational and Theoretical Nanoscience. 2019.

In addition, in research conducted by C. A. BATISTA we produce:

- C. A. BATISTA , **L. D. DA SILVA**, I. R. R. GONZÁLEZ, A. M. S. MACÊDO, W. R. DE OLIVEIRA, S. B. MELO. Quantum transport in curved surface. (Manuscript in preparation).

2 BRIEF REVIEW ON QUANTUM TRANSPORT

In this chapter, we give the formal general definition of retarded and advanced Green functions.

2.1 QUANTUM SCATTERING THEORY

Figure 1 – Physical system defined as a scattering region connected to two semi-infinite leads.

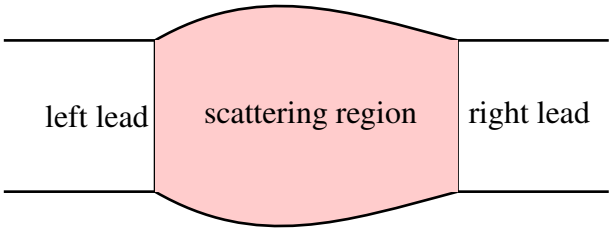

Source: (SILVA et al., 2019)

Consider a system composed of a scattering region connected to two semi-infinite leads, as shown in Figure 1. The wave function ψ of the scattered particle can be obtained by solving the time-independent Schrödinger equation

$$\left(-\frac{\hbar^2}{2m}\nabla^2 + V(\mathbf{r})\right) \cdot \psi(\mathbf{r}) = E\psi(\mathbf{r}), \tag{2.1}$$

where m is the mass of the particle, E is the incident energy and V is the potential function. The Green's function associated with the scattering problem is defined by the equation

$$[E - \mathscr{H}] \cdot G(\mathbf{r}, \mathbf{r}') = \delta(\mathbf{r} - \mathbf{r}'), \tag{2.2}$$

where δ is the Dirac delta function and the operator

$$\mathscr{H} := \left(-\frac{\hbar^2}{2m}\nabla^2 + V(\mathbf{r})\right) \tag{2.3}$$

is the Hamiltonian of the system.

In quantum scattering theory, knowing $G(\mathbf{r}, \mathbf{r}')$ with the appropriate boundary conditions one can compute all observables of physical interest. For instance, the transmission coefficient for particle transfer from the left lead to the right one can be calculated using the Landauer formula (DATTA, 2005; MEIR; WINGREEN, 1992):

$$T(E) = \mathrm{Tr}\left[\Gamma_L G^r(E) \Gamma_R G^a(E)\right], \tag{2.4}$$

where $G^{r,a}$ are the retarded and advanced Green's functions of the entire system respectively (including the coupling to the semi-infinite leads), and $\Gamma_{\{L,K\}}$ are the system-lead coupling functions. The coupling functions can be written as

$$\Gamma_k = i(\Sigma_k^r(E) - \Sigma_k^{r^\dagger}(E)), \tag{2.5}$$

where $k \in \{L,R\}$ and $\Sigma_k^r = u_k g_k^r(E) u_k^\dagger$ represents the self-energy matrix that describes the spectral effects of the coupling to the semi-infinite leads, $g_k^r(E)$ represents the Green's function of the k^{th} isolated semi-infinite leads, and u_k is the matrix that accounts for the coupling of the k^{th} lead to the scattering region. From its definition, the matrix Green's function must satisfy, $G^r = (G^a)^\dagger$, then, to calculate $T(E)$, we must solve the algebraic equation

$$[\varepsilon I - \mathscr{H} - \Sigma_L^r(E) - \Sigma_R^r(E)] \cdot G^r = I, \tag{2.6}$$

where $\varepsilon = E + i0^+$ and I is the identity matrix. Among the transport properties that can be computed from the solution of the scattering problem, we are particularly interested in the system's conductance, which is related to the transmission coefficient $T(E)$ by the Landauer formula (LANDAUER, 1989):

$$G_0 = g_0 T(E), \tag{2.7}$$

where $g_0 = \frac{2e^2}{h}$ is the conductance quantum.

Assuming that Γ_L and Γ_R are known, the problem of calculating the conductance is thus reduced to the computation of the Green's function G^r for a given incident energy E, as suggested in Eq. (2.4).

2.2 CALCULATING SELF-ENERGY

In this subsection, we will present a summary of the equations needed to calculate the self-energy matrices. The details of the statements for each formula are outlined in chapters 5 and 6 of (DOLLFUS PHILIPPE; TRIOZON, 2016).

For numerical calculations, we can represent the physical system by a 2D structured mesh with spacing equal to a. The stationary solutions of the Schrödinger equation in terms of the transverse modes is given as

$$\chi_p(i) = \sqrt{\frac{2}{M+1}} \sin\left(\frac{p\pi i}{M+1}\right), \tag{2.8}$$

where $M+1$ is number of mesh steps along y, $0 \leq i \leq M+1$, $p = 1,\ldots,M$, and $\chi_0(i) \equiv 0 \equiv \chi_{M+1}(i)$. The dispersion relations for this model is:

$$E_p(k) = V_L + E_p + 2t_0\left[1 - \cos\left(k_p a\right)\right]. \tag{2.9}$$

with

$$E_p = 2t_0\left[1 - \cos\left(\frac{p\pi}{M+1}\right)\right], \tag{2.10}$$

$$t_0 = -\frac{\hbar^2}{2ma^2} \tag{2.11}$$

and V_L is the potential in the left lead.

The self-energy matrix for the left lead is given by :

$$\Sigma_L^r(i,i',E) = \sum_{p=1}^{M} \chi_p(i)\chi_p(i')g_L^r(E), \tag{2.12}$$

where $g_L^r(E)$ is the one-dimensional lead Green's function expressed by

$$g_L^r(E) = \frac{(E + i0^+ - 2t_0 - V_L - E_p) + \sqrt{(E - i0^+ - 2t_0 - V_L - E_p)^2 - 4t_0^2}}{2t_0^2} \tag{2.13}$$

where, whatever the energy, the complex square root is chosen with negative imaginary part. From $\Sigma_L(E)$ one also obtains the $\Gamma_L(E)$ of Eq. 2.5:

$$\Gamma_L^r(i,i',E) = \sum_{\text{propagating modes p}} \chi_p(i)\chi_p(i')2t_0\sin(k_p a). \tag{2.14}$$

The wave vector k_p of mode p is given by:

$$k_p a = \arccos\left(1 - \frac{E - V_L - E_p}{2t_0}\right) \tag{2.15}$$

The matrices $\Sigma_R(E)$ and $\Gamma_R(E)$ are calculated using the Eqs. (2.9) - (2.15), with a potentially different potential V_R.

2.3 RECURSIVE TECHNIQUE

The recursive technique for calculating Green's functions is based on slicing the device into simpler subsystems, from which Green functions can be easily calculated. These subsystems are then coupled using the Dyson equation (for a demonstration of these formula, see Ref. (DATTA, 1997)):

$$G = g + gHG, \tag{2.16}$$

where G is the full Green's function, g is the Green's function for a disconnected system, and H describes the coupling between subsystems. In general, the idea is to break the system into N subsystems, where we assume that the g function of the isolated slice is known (see Figure 2). The subsystems are added one by one; thus, the total Green's function can be obtained recursively using Eq. 2.16.

Figure 2 – Slices scheme. Device connected to two semi-infinite leads, the device is divided and N subsystems and coupled to the left and right leads. Here, $H_{j,j+1}$, with $j = 0,\ldots,N+1$, is the coupling matrix between neighboring slices.

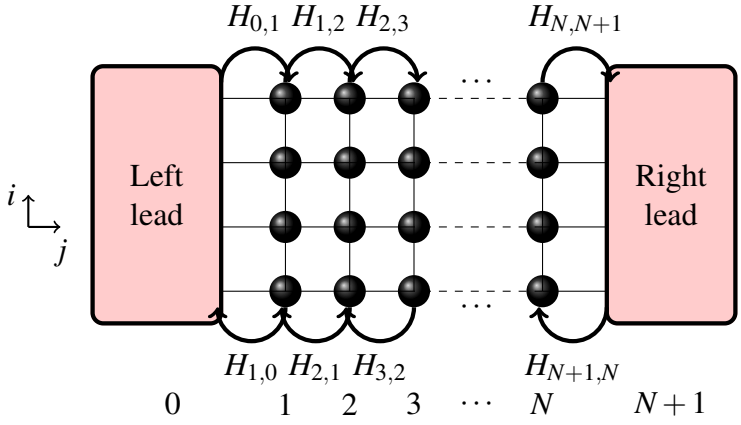

Source: The author (2019)

We will illustrate the use of Dyson's equation with an example. For this, suppose that the Green's function g_L describing the isolated semi-infinite left leads. Let's apply the Dyson equation to construct a Green's functions family that couples the device to the left lead. Consider a system consisting of two subsystems, would get $G^L_{1,2}$, i.e., elements of the Green's function between the first and last column of the coupled system. The first step is to couple the first column ($j = 1$) to the Green's function of the left lead. This can be done by projecting Eq. 2.16 between columns 0 and 1. Thus,

$$G^L_{1,1} = g_1 + g_1 H_{1,0} G^L_{0,1}. \tag{2.17}$$

To find the Green's function $G^L_{0,1}$, we apply the Dyson equation again

$$G^L_{0,1} = g_L H_{0,1} G^L_{1,1}, \tag{2.18}$$

where the function g is evaluated to zero since it is only set for slices isolated. Replacing (2.18) in (2.17), we get

$$G^L_{1,1} = (g_1 - H_{1,0} g_L H_{0,1})^{-1} \tag{2.19}$$

For column two ($j = 2$), the Green's function $G^L_{2,2}$ is given by

$$G^L_{2,2} = g_2 + g_2 H_{2,1} G^L_{1,2} \tag{2.20}$$

and

$$G^L_{1,2} = G^L_{1,1} H_{1,2} G^L_{2,2}. \tag{2.21}$$

Again, replacing (2.21) in (2.20) we get

$$G^L_{2,2} = \left(g_2 - H_{2,1} G^L_{1,1} H_{1,2}\right)^{-1}. \tag{2.22}$$

Proceeding as above, we can obtain the following recurrence relations:

$$G^L_{j,j} = \left(g_j - H_{j,j-1} G^L_{j-1,j-1} H_{j-1,j}\right)^{-1}, \tag{2.23}$$

$$G^L_{0,j} = G^L_{0,j-1} H_{j-1,j} G^L_{j,j}. \tag{2.24}$$

with $j = 2 \ldots N$.

The recursive technique is a convenient way to calculate specific Green's functions in large complex systems that can be divided into several connected subsystems. From the computational aspect, this recursive approach, for large systems, can be much faster than a direct solution of the Equation 2.6.

3 DISCRETE EXTERIOR CALCULUS

3.1 A BRIEF REVIEW OF EXTERIOR CALCULUS

3.1.1 Forms in $\mathbb{R}^n$

Let W be a vector space over the real numbers $\mathbb{R}$ and $\{e_i\}_{i=1}^n$ a basis of W. We first define a real-valued linear functional φ on W to be a linear transformation of elements of W to the real numbers $\mathbb{R}$, i.e., $\varphi : W \to \mathbb{R}$. Thus for $w_1, w_2 \in W$ and $a, b \in \mathbb{R}$,

$$\varphi(aw_1 + bw_2) = a\varphi(w_1) + b\varphi(w_2). \tag{3.1}$$

The collection of all linear functionals on W constitutes a vector space termed the dual space to W, denoted as W^*. The linear functionals $\phi^1, \phi^2, \ldots, \phi^n$ of W^* defined as the maps which extracts the i^{th} component of the vector constitutes the dual base of W^*. The set $\{\phi^i\}_{i=1}^n$ is in fact the dual basis of $\{e_i\}_{i=1}^n$ since

$$(\phi^i)(e_j) = \begin{cases} 0, & \text{se } i \neq j \\ 1, & \text{se } i = j. \end{cases} \tag{3.2}$$

Therefore, each elements $\omega \in W^*$ can be written as

$$\omega = \sum \alpha_i \phi^i, \tag{3.3}$$

where α_i are scalar-valued functions. These liner functionals are called forms from of degree 1 or simply 1-forms. For convenience we will adopt the notation $\Omega^1(W^\star)$ to refer the set of all 1-forms on W^*.

Give $w_1, w_2 \in W$ and $\varphi^1, \varphi^2 \in W^*$, we define a exterior product (or wedge product) between φ^1 and φ^2, denoted by $\wedge$, as

$$\varphi^1 \wedge \varphi^2(w_1, w_2) = \det(\varphi^i(w_j)) \tag{3.4}$$

Note that the exterior product is an alternate product (i.e., $\varphi^1 \wedge \varphi^2 = -\varphi^2 \wedge \varphi^1$) and bilinear (i.e., φ in linear in each of its arguments) consequently

$$\varphi \wedge \varphi = 0 \quad \text{for all} \quad \varphi \in W^* \tag{3.5}$$

and

$$(a\varphi_1 + b\varphi_2) \wedge \varphi_3 = a(\varphi_1 \wedge \varphi_3) + b(\varphi_2 \wedge \varphi_1), \text{ for } a, b \in \mathbb{R}. \tag{3.6}$$

The collection of all alternating bilinear functionals on W constitutes a vector space spanned by the set $\{\phi^i \wedge \phi^j, i < j\}$. Such space is often denoted by $\Omega^2(W^\star)$ and it's elements called forms of degree 2 or simply 2-forms on $W^\star$. Thus, each element $\omega \in \Omega^2(W^*)$ can be written as

$$\omega = \sum_{i<j} \alpha_{ij} \phi^i \wedge \phi^j \quad i, j = 1, \ldots, n, \tag{3.7}$$

where α_{ij} are scalar-valued functions.

To generalize the notion of higher-order forms we must highlight the exterior product can be extended to a large number of elements of the dual space setting

$$\varphi_1 \wedge \varphi_2 \wedge \ldots \wedge \varphi_k = \det(\varphi^i(w_j)), \quad i,j = 1,\ldots k. \tag{3.8}$$

It follows from the properties of determinants that $\varphi^1 \wedge \varphi^2 \wedge \ldots \wedge \varphi^k$ is in fact k-liner and alternate. An k-forms can be thought of as elements of the vector space $\Omega^k(W^\star)$ spanned by set

$$\{\phi^{i_1} \wedge \ldots \wedge \phi^{i_k}; \quad i_1 < \ldots < i_k, \quad i = 1,\ldots,n\}. \tag{3.9}$$

Therefore, each element $\omega \in \Omega^k(W^\star)$ can be written as

$$\omega = \sum_{i_1<\ldots<i_k} \alpha_{i_1\ldots i_k}(\phi^{i_1} \wedge \ldots \wedge \phi^{i_k}), \quad i_j \in \{1,\ldots,n\}, \tag{3.10}$$

where $\alpha_{i_1\ldots i_k}$ are scalar-valued functions. When appropriate, we will denote by I the k-upla $(i_1,\ldots,i_k)$, $i_1 < \ldots < i_k$, $i_j \in \{1,\ldots,n\}$, and will user the following notation for ω:

$$\omega = \sum_I \alpha_I \phi^I. \tag{3.11}$$

We also set the convention that $\Omega^0(W^*)$ is the space of scalar-valued functions called 0-forms.

For each $p \in \mathbb{R}^n$ the set $\mathbb{R}^n_p = \{p - q : q \in \mathbb{R}^n\}$ is a vector space called tangent space of $\mathbb{R}^n$ in p. A basis for its dual space $(\mathbb{R}^n_p)^*$ is obtained by taking $(dx^i)_p$, $i = 1\ldots n$, where $x^i : \mathbb{R}^n \to \mathbb{R}$ is the map which extracts the i^{th}-coordinate of each point. It's possible to show that all linear functionals $(dx^i)_p$ satisfy (3.2) and therefore are dual for tangent space $\mathbb{R}^n_p$ (see proof in (MANFREDO, 1976)). Thus, in space $\mathbb{R}^n$ the expression (3.11) in terms of theses basis is written as

$$\omega = \sum_I \alpha_I dx^I. \tag{3.12}$$

Example 3.1.1. A 1-form in $\mathbb{R}^3$:

$$\omega = \alpha_1 dx^1 + \alpha_2 dx^2 + \alpha_3 dx^3.$$

Example 3.1.2. A 2-form in $\mathbb{R}^3$:

$$\omega = \alpha_{12} dx^1 \wedge dx^2 + \alpha_{13} dx^1 \wedge dx^3 + \alpha_{23} dx^2 \wedge dx^3.$$

3.1.2 Exterior derivative

For any differentiable function $f \in \Omega^0(W^*)$ the usual differential of the function f is the 1-form

$$df = \sum_i \frac{\partial f}{\partial x_i} dx^i. \tag{3.13}$$

The exterior derivative, denoted as d, is an operation that transforms a k-form ω into a $(k+1)$-form $d\omega$ by simple operation defined in (3.13) applied to the scalar-valued components of the form. More precisely, if $\omega = \sum_I \alpha_I dx^I$ is a form in $\mathbb{R}^n$ the exterior derivative operator $d\omega$ of ω is defined by

$$d\omega = \sum_I d\alpha_I \wedge dx^I. \tag{3.14}$$

Give an arbitrary k-form ω_1 and s-form ω_2, the exterior derivative operator satisfies the following properties:

$$d(\omega_1 + \omega_2) = d\omega_1 + d\omega_2, \tag{3.15}$$

$$d(\omega_1 \wedge \omega_2) = d\omega_1 \wedge \omega_2 + (-1)^k \omega_1 \wedge d\omega_2, \tag{3.16}$$

$$d(\mathrm{d}\omega_1) = 0. \tag{3.17}$$

Example 3.1.3. Consider a 1-form $\omega = xyzdx + yzdy + (x+z)dz$ in $\mathbb{R}^3$. Then, using (3.13), (3.14), (3.15) and the properties (3.4) – (3.6) we get

$$d\omega = d(xyz) \wedge dx + d(yz) \wedge dy + d(x+y) \wedge dz \tag{3.18}$$

$$= (yzdx + xzdy + xydz) \wedge dx + (zdy + ydz) \wedge dy + (dx + dz) \wedge dz \tag{3.19}$$

$$= -xzdx \wedge dy + (1-xy)dx \wedge dz - ydy \wedge dz. \tag{3.20}$$

In the language of differential forms, the **Stokes's Theorem** in $\mathbb{R}^3$ says that the integral of a differential form ω over the boundary of some orientable surface S is equal to the integral of its exterior derivative $d\omega$ over the whole of S, i.e.

$$\int_S \mathrm{d}\omega = \int_{\partial S} \omega. \tag{3.21}$$

The operation exterior derivative can be thought of as a generalization of the differential of a function.

3.1.3 Hodge star

The Hodge star operator is a linear mapping from k-forms to $(n-k)$-forms, denoted as $* : \Omega^k \to \Omega^{n-k}$. The Hodge star transforms each subspace spanned by $dx^{i_1} \wedge \ldots \wedge dx^{i_k}$ to an element of the orthogonal subspace, i.e.,

$$*(dx^{i_1} \wedge \ldots \wedge dx^{i_k}) = (-1)^\sigma (dx^{j_1} \wedge \ldots \wedge dx^{j_{n-k}}), \tag{3.22}$$

where the ordering of indices from $i_1 < \ldots < i_k$, $j_1 < \ldots < j_{n-k}$, $(i_1, \ldots, i_k, j_1, \ldots, j_{n-k})$ is a permutation of the integers $1, 2, \ldots, n$, and σ is 0 or 1 according to permutation is even or odd, respectively. So for example, if we consider the basic 1-forms dx^i in $\mathbb{R}^3$, then

$$*dx^1 = dx^2 \wedge dx^3, \tag{3.23}$$

$$*dx^2 = dx^1 \wedge dx^3, \tag{3.24}$$

$$*dx^3 = dx^1 \wedge dx^2. \tag{3.25}$$

Example 3.1.4. If $\omega = \alpha_1 dx^1 + \alpha_2 dx^2$ is a 1-form in $\mathbb{R}^2$, then

$$*\omega = \alpha_1 dx^2 - \alpha_2 dx^1 \tag{3.26}$$

Example 3.1.5. If $\omega = \alpha_{12} dx^1 \wedge dx^2 + \alpha_{13} dx^1 \wedge dx^3 + \alpha_{23} dx^2 \wedge dx^3$ is a 2-form in $\mathbb{R}^3$ then

$$*\omega = \alpha_{12} dx^3 - \alpha_{13} dx^2 + \alpha_{23} dx^1. \tag{3.27}$$

The differential operators in vector calculus can be seen as special cases of the exterior derivative and the Hodge star acting on a form of a particular degree. In Table 1 we describe the gradient (grad), curl and divergent (div) in local coordinates and in exterior calculus notation.

Table 1 – In Cartesian coordinates of $\mathbb{R}^3$, $f(x,y,z)$ is a scalar field and $\upsilon = (A,B,C)$ is a vector field. In exterior calculus notation (third column), the f and F fields are differentiable forms related to the f and υ fields by $F = f^\flat$, $\omega = \upsilon^\flat$. The $\flat$ operator converts a vector to a 1-form.

Symbol	Vector calculus ($\mathbb{R}^3$)	Exterior calculus
$\operatorname{grad} f$	$\frac{\partial f}{\partial x}dx + \frac{\partial f}{\partial y}dy + \frac{\partial f}{\partial z}dz$	dF
$\nabla \times \upsilon$	$\left(\frac{\partial C}{\partial y} - \frac{\partial B}{\partial z}\right)dx \left(\frac{\partial C}{\partial x} - \frac{\partial A}{\partial z}\right)dy + \left(\frac{\partial B}{\partial x} - \frac{\partial A}{\partial y}\right)dz$	$*d\omega$
$\operatorname{div} \upsilon$	$\frac{\partial A}{\partial x} + \frac{\partial B}{\partial y} + \frac{\partial C}{\partial z}$	$*d*\omega$

Source: adapted from (NESTLER et al., 2018)

3.1.4 Laplace-Beltrami

The Laplace-Beltrami operator, often denoted by ∇^2, is the generalization of the Laplacian to curved spaces. Therefore, it is used to operate on functions defined on surfaces in Euclidean space and, more generally, on Riemannian manifolds. The Laplace-Beltrami operator, like the Laplacian, is the divergence of the gradient. The formula for ∇^2 when applied to a scalar function φ is, in local coordinate

$$\nabla^2 \varphi = \frac{1}{\sqrt{|g|}} \frac{\partial}{\partial x_i} (\sqrt{|g|} g^{ij} \frac{\partial}{\partial x_i} \varphi), \tag{3.28}$$

where g is a metric.

How we know to write div, grad using exterior calculus (see Table 1), the Laplace-Beltrami operator for 0-forms can be expressed by

$$\nabla^2 := *d*d. \tag{3.29}$$

3.1.5 Manifolds

A general manifold is a topological space that is locally Euclidean. For instance, curve, plane, and sphere are all common examples manifolds. More precisely, an n-dimensional manifold (in $\mathbb{R}^n$) is a subset M of $\mathbb{R}^n$ together with an of a collection homeomorphisms to Euclidean space called charts. These charts must be compatible such that the composition of a chart with the inverse of an overlapping chart must also be a homeomorphism, and this homeomorphism is termed the transition map. In order for the manifold to be suitable for calculus, it must be a differentiable manifold the which requires that the transition maps be differentiable. The notion of forms in a manifold can be extend using similar considerations for forms in space $\mathbb{R}^n$, see (SPIVAK, 1965; MANFREDO, 1976).

3.2 DISCRETE EXTERIOR CALCULUS

In this section, we present a brief description of the main tools of the DEC discretization procedure. The discretization domain, the differential forms and operators will be presented in detail. A more thorough presentation of the mathematical fundamentals of DEC can be found in Refs. (DESBRUN; KANSO; TONG, 2008; HIRANI, 2003). For a careful description of the discrete exterior calculus objects and their implementations, see (BELL; HIRANI, 2012; ELCOTT; SCHRODER, 2006; MOHAMED; HIRANI; SAMTANEY, 2016b). For a review on exterior calculus on manifolds, see (SPIVAK, 1965).

3.2.1 Discrete domain

A simplicial complex $\mathscr{K}$ in R^N is a collection of simplices in R^n such that

1. Every face of a simplex of $\mathscr{K}$ is in $\mathscr{K}$.
2. The intersection of any two simplices of $\mathscr{K}$ is either a face of each of them or it is empty.

In DEC, the continuous spatial domain of dimensions $n = 2,3$ is approximated by a simplicial complex $\mathscr{K}$, which is a manifold that admits a metric and is orientable (MUNKRES, 1984). Here, the simplices (nodes, edges and triangles) of $\mathscr{K}$ are denoted by σ^k, where the superscript index indicates the dimension of the simplex. For instance, in a 2D domain, σ^0, σ^1 and σ^2 represent the nodes (0-simplex), edges (1-simplex) and triangles (2-simplex) of $\mathscr{K}$, respectively. Here, we will refer to a simplicial complex simply by a primal mesh $\mathscr{K}$ and denote by N_k the number of its k-simplex.

From a primal mesh $\mathscr{K}$ one can construct a dual mesh $\star\mathscr{K}$ through the Voronoi duality (circumcentric duality). Therefore, the dual mesh can be defined via the location of the circumcenter of each triangle of the primal mesh with the connectivity induced by the primal connectivity (see Figure 3). For each k-simplex $\sigma^k \in \mathscr{K}$, its dual is a $(n-k)$-cell, which we denote as $\star\sigma^k \in \star\mathscr{K}$. Geometrically, 0-cells associated with the triangular faces are the circumcenters

of the triangles. The 1-cells associated with one of the primal edges are the orthogonal line segments that connect the circumcenters of the triangles to their related primal edges, whereas 2-cells (polygons) associated with primal nodes are formed by the dual of the edges connected to this primal nodes (see Figure 5). This article focuses on simplicial meshes over a flat/curved surface, and therefore the simplices/cells involved are restricted to nodes, edges, triangle, and their respective duals. The orientation of each element needs to be specified and must remain consistent throughout all the mathematical operations. Here, the positive orientation of both triangles and polygons are assumed to be counterclockwise. The orientation of the dual edges can be defined by rotating the primal edge orientation (arbitrarily defined) 90 degrees along the orientation of the triangle. In Figure 3 we shown an example of a primal and its dual two-dimensional mesh. For a 3D mesh representing a curved surface, the dual edges can be twisted lines and the dual cells can be non-planar.

Figure 3 – Example of a simplicial complex and its dual. The elements of the primal mesh (k-simplices) are shown in black lines, while elements of the dual mesh ((n-k) -cell) are represented by red dashed lines.

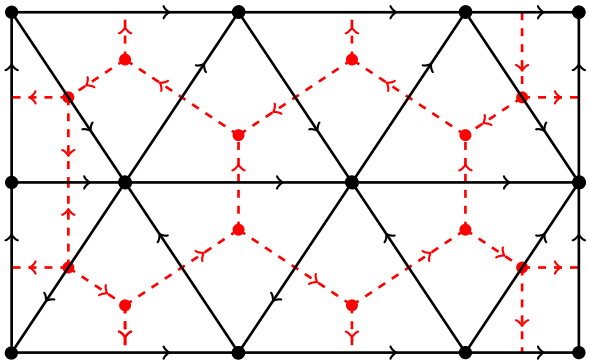

Source: (SILVA et al., 2019)

3.2.2 Discretization of differential forms

The fundamental objects of the DEC method are the discrete representatives of the continuous differential forms. Given a k-form ω in $\mathbb{R}^n$, a k-discrete form (denoted by $\bar{\omega}$) is a column matrix of dimension $N_k \times 1$ whose entries are given by a real number assigned to each $\sigma_i^k \in \mathscr{K}$ through the relation

$$\bar{\omega}_i = \int_{\sigma_i^k} \omega, \qquad i = 1, \cdots, N_k. \tag{3.30}$$

In terms of algebraic topology, the paths formed by a linear combination of k-simplices σ^k are called k-chains (see Figure 5) and the integral over these "paths", i.e., the discrete forms of dimension k, are called a primal k-cochain or simply a k-cochain (MUNKRES, 1984). By convention the integral of a continuous 0-form ω over 0-dimensional objects is simply the value of a form (continuous function) at the point, i.e., $\bar{\omega}_i = \omega(\sigma_i^0)$.

Discrete forms can also be defined in a dual mesh. In this case, we may refer to the discrete forms of dimension k as a dual k-cochain. Here, we will represent the space of primal

k-cochain and dual k-cochain by $\mathscr{C}^k(\mathscr{K})$ and $\mathscr{D}^k(\star\mathscr{K})$, respectively. Such spaces are related via the discrete exterior derivative and Hodge star operators as we will show in the following subsections.

3.2.3 Discrete boundary operator

The k^{th} discrete boundary operator, denoted by ∂_k takes a k-chain to its $(k-1)$-chain boundary. It is defined by its action on an oriented k-simplex $\sigma^k = \{p_0, p_1, ..., p_k\}$:

$$\partial_k \sigma^k = \partial_k \{p_0, p_1, ..., p_k\} := \sum_{j=0}^{k} (-1)^j \{p_0, p_1, ..., \hat{p}_j, ..., p_k\} \tag{3.31}$$

where $\hat{p}_j$ indicates that the j^{th} term is omitted. To illustrate it's action on a simplex we consider a triangle oriented $\sigma^2 = \{p_1, p_2, p_3\}$. The boundary of σ^2, by the above definition, is the chain $\{p_1, p_2\} - \{p_0, p_2\} + \{p_1, p_2\}$, which are the three boundary edges of the triangle. Since the boundary operator is a linear map from k-chain to $(k-1)$-chain, it can simply be represented by matrix of size $N_{k-1} \times N_k$ so that the action of ∂_k on a k-chain is the usual matrix multiplication.

3.2.4 Discrete exterior derivative

The k^{th} discrete exterior derivative, denoted by $d_k : \mathscr{C}^k(\mathscr{K}) \longrightarrow \mathscr{C}^{k+1}(\mathscr{K})$, is a linear map that transforms a k-cochain into a $(k+1)$-cochain through the relation $d_k = \partial^T$ (see Figure 5), where ∂ is the boundary operator acting on simplices (see (MUNKRES, 1984)). In practical terms, the discrete k-dimensional exterior derivative operator (reference to the k-cochain dimension) is the incidence matrix (with sign) between σ^{k+1} and σ^k of $\mathscr{K}$ (the signal is determined by relative orientation of the simplices). Therefore, d_k is a sparse $N_{k+1} \times N_k$ matrix whose nonzero elements are 1 and -1. For example, the discrete exterior derivative operator acting on nodes of a 2D mesh is an $N_1 \times N_0$ matrix defined by

$$(d_0)_{ij} = \begin{cases} +1, & \text{if } j \text{ is the ending node of edge } i, \\ -1, & \text{if } j \text{ is the starting node of edge } i, \\ 0, & \text{otherwise.} \end{cases} \tag{3.32}$$

The discrete exterior derivative operator acting on k-cochains in the dual mesh is defined by the relation $\bar{d}_k = (-1)^k d_{k-1}^T$. However, the DEC version for Stokes's theorem is given by

$$\int_{\sigma^{k+1}} d_k \bar{\omega}^k = \int_{\partial \sigma^{k+1}} \bar{\omega}^k, \tag{3.33}$$

where $\partial \sigma^{k+1}$ is the k-chain boundary of σ^{k+1}.

3.2.5 Discrete Hodge star operator

The k^{th} discrete Hodge star denoted by $*_k : \mathscr{C}^k(\mathscr{K}) \longrightarrow \mathscr{D}^{k-1}(\star\mathscr{K})$ is linear map that transforms primal k-cochains into dual $(n-k)$-cochains (see Figure 5). The DEC approach admits several interpretations for the discrete Hodge star operator (MOHAMED; HIRANI; SAMTANEY, 2016a). Conveniently, we will use the Hodge circumcentric operator which is represented by a diagonal matrix $N_k \times N_k$ defined by

$$(*_k)_{ii} := \frac{|\star\sigma_i^k|}{|\sigma_i^k|}, \tag{3.34}$$

where $|\cdot|$ indicates the primal and dual volume of the elements. For example, $|\sigma^1|$ represents the length of the edge σ^1 and $|\star\sigma^0|$ the face area of the dual cell $\star\sigma^0$. By conversion the volume of a 0-simplex is equal to one. As described in (MOHAMED; HIRANI; SAMTANEY, 2016b), in the 3D mesh of a curved surface the length of a dual edge is its length as a twisted line. On the other hand, for each primal node, its dual is the non-planar polygon consisting of sector contributions from all flat triangles sharing the primal node, and its area is calculated accordingly as a non-planar surface area.

The maps dual of $(n-k)$-cochains to primal k-cochains is realized by the inverse operator $*^{-1}$ (see Figure 5), which is the inverse of the matrix defined in Eq. (3.34).

The DEC approach admits other interpretations for the discrete Hodge star operator, the most common being the Galerkin (BOSSAVIT, 1998) and barycentric definitions (AUCHMANN; KURZ, 2006; TREVISAN; KETTUNEN, 2004). However, the Galerkin and the barycentric definitions lead to sparse non-diagonal representations, which implies a higher computational cost, in comparison with the diagonal definitions based on circumcentric duals (MOHAMED; HIRANI; SAMTANEY, 2016a), without significant gains in accuracy (MOHAMED; HIRANI; SAMTANEY, 2018). Such alternative definitions would make our recursive method proposed in Subsection 4.1.2 a challenging task, to say the least.

3.2.6 Volume of circumcentric dual cells

The choice for the dual mesh, built through the circumcentric duality, is motivated by resulting in a diagonal matrix representation for the Hodge star operator. As suggested by the Equation (3.34), each nonzero element of this matrix depends on the volume of the primal and dual mesh elements. In general, the calculation of the volume of primal elements is simple, so we will focus on presenting the possibilities of calculating the volume of circuncentric dual cells. The correct setting for such volume is crucial for the correct definition of the discrete Hodge star operator. In this subsection, we will exemplify the use of the sign convention, established in (HIRANI; KALYANARAMAN; VANDERZEE, 2013), for the volume of dual cells. Numerical evidence suggests that such convention enables DEC to work correctly with Delaunay and non-Delaunay meshes, using the diagonal definition of the Hodge star operator (MOHAMED; HIRANI; SAMTANEY, 2018).

Figure 4 – (a) Delaunay mesh where c, p and A denote circumcenters, vertices and parts of the dual areas to the vertex p_0, respectively. The notation $d_{i,j}$ refers to the distance between the circumcenters c_i and c_j, while $d_{0,j}$ indicates the distance between I_0 and c_j. (b) Delaunay mesh. (c) Non-Delaunay mesh.

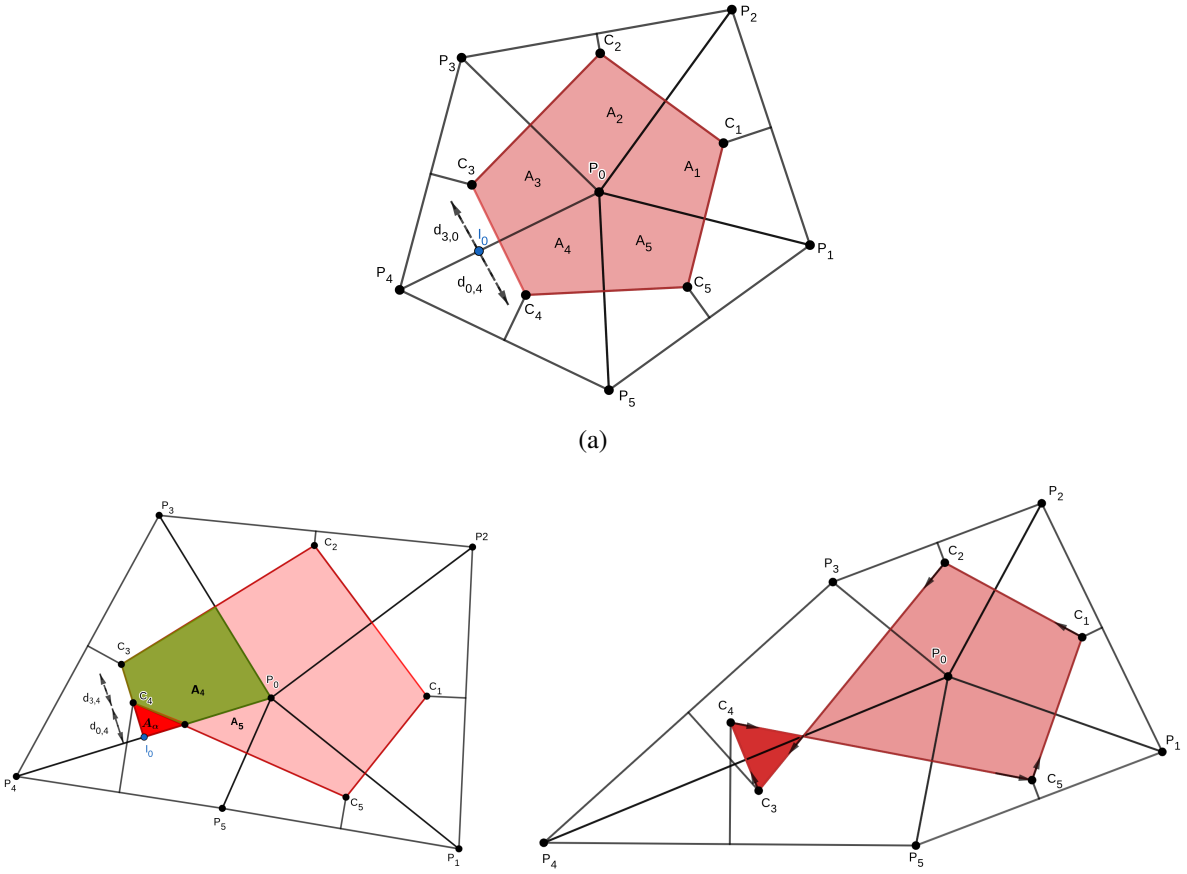

Source: The author (2019)

Figure 5(a), illustrate a typical 2D mesh, where all the circumcenters are within their associated triangles. In this case, dual edges such as $\star\{p_0, p_4\}$, are composed of two dual components of two neighboring triangles ($\{p_0, p_4, p_5\}$ and $\{p_0, p_3, p_4\}$), while dual face elements (for example, shaded regions), consists of several parts from triangles sharing the same primal vertex. For example, dual face $\star\{p_0\}$ is composed by 5 parts $A_1, \ldots, A_5$. In this case, we can get the length of the dual edge $\star\{p_1, p_4\}$ simply by summing the length of each component, i.e., $|\star\{p_0, p_4\}| = d_{3,0} + d_{0,4}$, as illustrated in the Figure 5(a). On the other hand, the area of red shaded 2-cell by summing over all its five parts, i.e., $|\star\{p_0\}| = \sum_i^5 |A_i|$. Note that, for such meshes, the volumes of circumcentric dual cells are obviously positive.

Figure 5(b) shows an example of a Delaunay mesh in which the circumcenter (c_4) is outside the triangle associated ($\{p_0, p_4, p_5\}$). Then, $|\star\{p_1, p_4\}| = d_{3,4} = d_{3,0} - d_{0,4}$. It is noted that volume of dual edge $\star\{p_3, p_4\}$, is still positive, although the sign of $d_{0,4}$ be negative (HIRANI; KALYANARAMAN; VANDERZEE, 2013). For this specific case, the calculation for the volume of dual face is unaffected and therefore follows as previously defined, summing the area of all red

shaded regions.

Figure 5(c), shows a sample non-Delaunay mesh with circumcenters c_3 and c_4 both outside their associated triangles ($\{p_0, p_4, p_5\}$ and $\{p_0, p_3, p_4\}$, respectively). According to the convention (HIRANI; KALYANARAMAN; VANDERZEE, 2013) the dual edge $\star\{p_0, p_4\}$ has a negative volume, since it is oriented in the opposite direction to the orientation induced by the primal edge (90° counterclockwise in relation to their primal edges). Still in Figure 5(c), as established by (HIRANI; KALYANARAMAN; VANDERZEE, 2013), the dual cell area of $\star\{p_0\}$ can be found to be the difference between right light red region (counterclockwise oriented) and left dark red region (clockwise oriented). These are examples of signed volumes.

3.2.7 Discrete Laplace-Beltrami

The discrete Laplace-Beltrami operator on a k-cochain is given by

$$\nabla^2 := (-1)^{nk+1} *_k^{-1} d_k^T *_{k+1} d_k, \tag{3.35}$$

in which, n is the dimension of the discrete domain and $0 < k < n$. Making $k = 0$ and $n = 3$ in Eq. (3.35) we have the discretization of the Laplacian scalar in $\mathbb{R}^3$:

$$\nabla^2 = \frac{\partial^2}{\partial x^2} + \frac{\partial^2}{\partial y^2} + \frac{\partial^2}{\partial z^2}. \tag{3.36}$$

Figure 5 – In the first line, the primal elements of a 2D mesh and in the second line their corresponding dual elements. In the horizontal, the derivative operator maps k-cochain to $(k+1)$-cochain, whereas in the vertical direction the Hodge star operator and its inverse mapping between primal k-cochain and dual $(n-k)$-cochain. (color online)

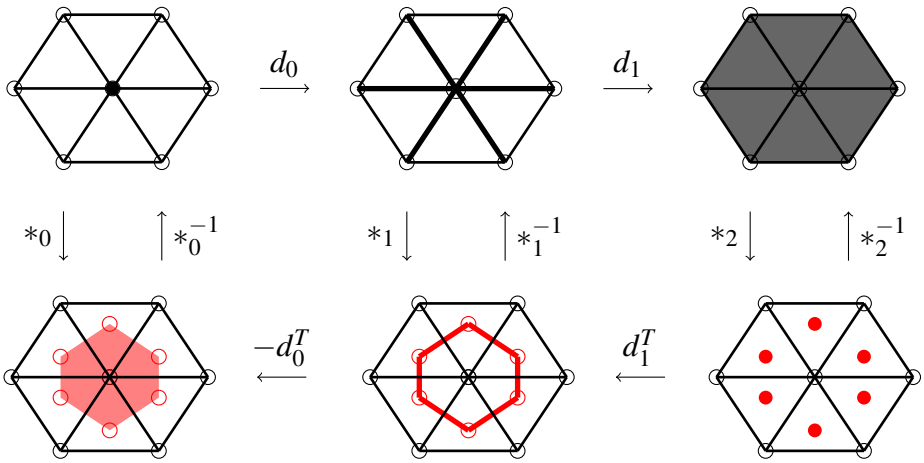

Source: (SILVA et al., 2019)

3.2.8 Example calculation

To clarify the ideas, we will illustrate how to calculate these operators. We will now produce the matrices that represented the discrete operators acting on the two-dimensional triangle oriented

$\sigma^2 = \{p_0, p_1, p_2\}$, with nodes p_0, p_1 and p_2 at $(0,0)$, $(1,0)$ and $(0.5,1)$, respectively. This example, edges are oriented so that they point toward the node index of greater value and the face counterclockwise, as shown Figure 7(a). Their corresponding dual cells are obtained by taking the circumcentric dual of σ^2. Figures 6(b)-(c) illustrate primal and dual elements color-coded to represent the dual relationship between the elements in the primal and dual mesh.

Figure 6 – (a) The orientation of a triangle. (b) Primal elements. (c) Dual elements.

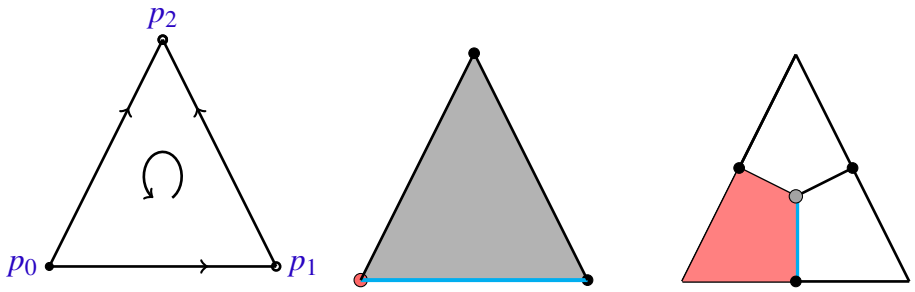

Source: (SILVA et al., 2019)

The discrete exterior derivative, which acts on 0-cochain it can be thought of as the signed matrix of incidence between edges and vertices of an oriented triangle. Similarly, the discrete exterior derivative, which acts on 1-cochain, is the signed matrix of incidence between oriented faces and edges. Thus, according to Figure 7(a):

$$d_0 = \begin{bmatrix} -1 & 1 & 0 \\ -1 & 0 & 1 \\ 0 & -1 & 1 \end{bmatrix}, \qquad d_1 = \begin{bmatrix} 1 & -1 & 1 \end{bmatrix}. \tag{3.37}$$

According to the definition of the Hodge star operator based on the circumcentric duality and summarized in Eq. (3.34), the Hodge star matrices $*_0$ and $*_1$ which act on 0-cochain and 1-cochain are:

$$*_0 \approx \begin{bmatrix} 0.17 & 0 & 0 \\ 0 & 0.17 & 1 \\ 0 & 0 & 0.15 \end{bmatrix}, \qquad *_1 \approx \begin{bmatrix} 0.375 & 0 & 0 \\ 0 & 0.25 & 0 \\ 0 & 0 & 0.25 \end{bmatrix}. \tag{3.38}$$

To calculate the DEC version of Laplace-Beltrami which act on 0-cochain, we use Eq. (3.35) with n = 2 and k = 0. Hence $L_0 = -*_0^{-1} d_0^T *_1 d_0$ yielding the matrix

$$L_0 \approx \begin{bmatrix} -3.67 & 2.20 & 1.47 \\ 2.20 & -3.67 & 1.470 \\ 1.66 & 1.66 & -3.33 \end{bmatrix}. \tag{3.39}$$

We present here how to compute the discrete operators acting on a simple triangle using the notation of the discrete exterior calculus. It is important to note that the Hodge star operator depends on geometry. Therefore, the choice of mesh type directly influences the discrete Laplace-Beltrami operator configuration. For our proposal, we will choose a structured mesh composed of isosceles rectangle triangles. We will see later that this choice promotes a change in the Hodge star operator so that the discrete Laplace-Beltrami, when subjected to the boundary conditions of Dirichlet, is a sparse and tridiagonal matrix. In addition to the gain in storage efficiency, it allows the use of efficient algorithms to compute the desired Green's functions. On the other hand, it is noteworthy that the choice of a uniform triangular mesh is convincing to our problem but it is not reasonable for a DEC approach, for instance, of equations governing fluid dynamics. In this context, the dual circumcenter would generate a singular matrix $\star_1$ since the circumcentric line would lie on the opposite edge of the right angle.

4 GREEN'S FUNCTION

4.1 DISCRETE GREEN'S FUNCTION

In this section, we will show how to use the DEC scheme to calculate the retarded Green's functions G^r. In the first subsection, the discretization of full retarded Green's functions is carried out following the model described in (DATTA, 2005) but replacing the standard numerical discretization by the DEC approach. In the second subsection, we begin with the three-dimensional DEC discretization of Schrödinger equation and then introduce a technique, based on the efficient recursive Green's function (RGF) method (THOULESS; KIRKPATRICK, 1981), to calculate the conductance of a curved sample.

The curved system adopted here are discretized by a simplicial mesh consisting of flat triangles connecting the primal nodes, where each of the primal nodes are positioned on a smooth surface. The surface S is the result of the deformation in vertical direction of a structured-triangular mesh D (consisting of isosceles right triangles) through a smooth application φ, as illustrated in Figure 7. The resulting triangulation is a curved non-Delaunay mesh. Previous investigation (MOHAMED; HIRANI; SAMTANEY, 2018) showed that DEC solutions using circumentric dual and the diagonal Hodge star definitions produce correct numerical solutions even with non-Delaunay triangulations. For instance, the simulation of an inviscid incompressible flow over a non-Delaunay triangulation of a sinusoidal curved surface (generated similar to S) showed insignificant differences between the Delaunay and the non-Delaunay triangulations. According to the authors, it is essential to correctly consider the signed volume for some flipped dual edges and overlapping dual cells that are present in these meshes (see Subsection 3.2.6). Such convention for signed volumes is essential to represent the discrete Hodge star operator in non-Delaunay meshes correctly. The sign convention is discussed in detail in (HIRANI; KALYANARAMAN; VANDERZEE, 2013).

Figure 7 – Embedding of a two-dimensional surface in three-dimensional space.

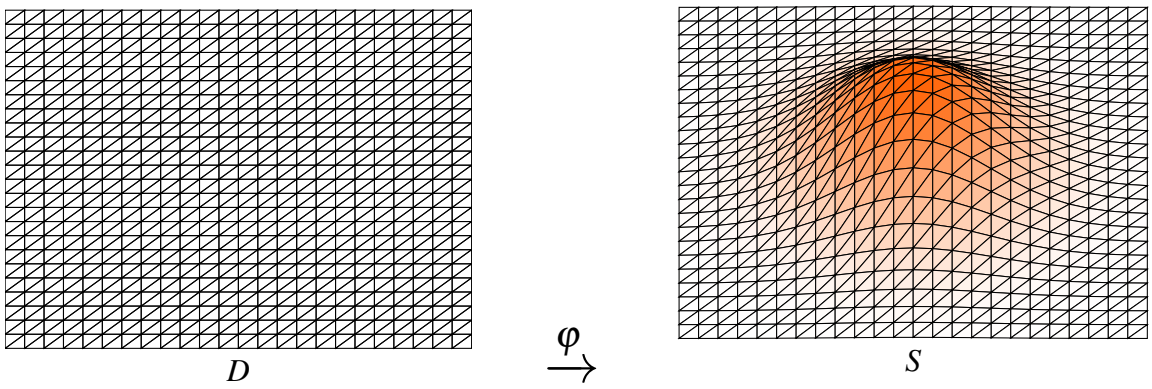

Source: (SILVA et al., 2019)

4.1.1 Full retarded Green's function

This discretization was prepared by adapting the procedure used by CHEN; CHEW when presenting discrete Green's functions of a wave equation (CHEN; CHEW, 2017a). In discrete exterior calculus the potential function $V(\mathbf{r})$ (Eq. (2.1)) is treated as a $N_0 \times 1$ column array (0-cochain) defined by

$$\bar{V} = \begin{pmatrix} \bar{V}_1 \\ \vdots \\ \bar{V}_{N_0} \end{pmatrix}, \qquad \bar{V}_i \equiv V(\sigma_{\mathbf{i}}^{\mathbf{0}}). \tag{4.1}$$

According to the Eq. (3.35) the Schrödinger's Hamiltonian can be written as a $N_0 \times N_0$ matrix

$$\bar{\mathscr{H}} = \left(\frac{\hbar^2}{2m} \left(*_0^{-1} \mathrm{d}_0^T *_1 \mathrm{d}_0 \right) - \bar{U} \right), \tag{4.2}$$

where $\bar{U}$ is a diagonal matrix whose main diagonal is formed by $\bar{V}$, i.e, $\bar{U} = \mathrm{diag}(\bar{V})$.

In Eq. (2.2), for each given $\mathbf{r}'$, $G(\mathbf{r}, \mathbf{r}')$, in DEC notation, is treated as a $N_0 \times 1$ column array (0-cochain). Since r' has N_0 possibilities of choices, Green's function $G(\mathbf{r}, \mathbf{r}')$ can be considered as a $N_0 \times N_0$ matrix $\bar{G}$. Analogously, for any given $\mathbf{r}'$, the Dirac delta function $\delta(\mathbf{r}, \mathbf{r}')$ is treated as a $N_0 \times 1$ column array (2-cochain) which has value 1 if $\mathbf{r} = \mathbf{r}'$ and zero otherwise. Therefore, a discrete Dirac delta function can be replaced by a $N_0 \times N_0$ identity matrix. The Green's function is then the solution of equation

$$\left[E\bar{I} + \frac{\hbar^2}{2m} \left(*_0^{-1} \mathrm{d}_0^T *_1 \mathrm{d}_0 \right) - \bar{U} \right] \cdot \bar{G} = \bar{I}. \tag{4.3}$$

The Dirichlet boundary condition is implemented in Eq. (4.3) simply by assigning the value zero on all entries referring to primal nodes of the surface mesh boundary. Therefore,

$$\bar{G} = \left[E\bar{I} + \frac{\hbar^2}{2m} \left(*_0^{-1} \mathrm{d}_0^T *_1 \mathrm{d}_0 \right) - \bar{U} \right]^{-1} \tag{4.4}$$

is the discrete solution of Green's function in an surface mesh.

Assuming that the Green's functions on the left and right leads are known, the full retarded Green's function $\bar{G}^r$ can be expressed as

$$\bar{G}^r = \left[\varepsilon\bar{I} + \frac{\hbar^2}{2m} \left(*_0^{-1} \mathrm{d}_0^T *_1 \mathrm{d}_0 \right) - \bar{U} - \bar{\Sigma}_L - \bar{\Sigma}_R \right]^{-1}, \tag{4.5}$$

where

$$\bar{\Sigma}_L = \begin{pmatrix} \Sigma_L^r & 0 & \dots & 0 \\ 0 & 0 & \vdots & 0 \\ \vdots & \dots & \ddots & \vdots \\ 0 & \dots & \dots & 0 \end{pmatrix}_{N_0 \times N_0}, \qquad \bar{\Sigma}_R = \begin{pmatrix} 0 & 0 & \dots & 0 \\ 0 & 0 & \vdots & 0 \\ \vdots & \dots & \ddots & \vdots \\ 0 & \dots & \dots & \Sigma_R^r \end{pmatrix}_{N_0 \times N_0}. \tag{4.6}$$

Note that a solution for $\bar{G}^r$ would correspond to the inversion of an $N_0 \times N_0$ matrix, where N_0 is the number of nodes in the system. Therefore, is not efficient to evaluate directly the full retarded Green's function, $\bar{G}^r$, in large systems. In the next subsection, we will show the DEC version of the tight-binding representation of the system's Hamiltonian, and then recursively build the full retarded Green's function.

4.1.2 The DEC recursive technique for the Green's functions

Figure 8 – Voronoi cell. The dual 2-cell $\star p_{i,j}$ is marked dashed lines.

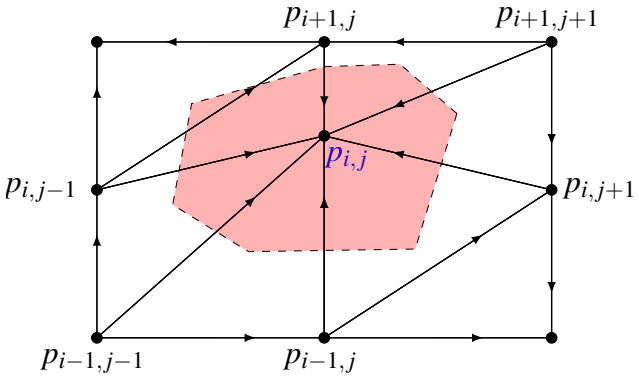

Source: (SILVA et al., 2019)

We start by considering the Schrödinger equation in three-dimensional space, which is given by

$$\left(-\frac{\hbar^2}{2m} \left(\frac{d^2}{dx^2} + \frac{d^2}{dy^2} + \frac{d^2}{dz^2} \right) + V(x,y,z) \right) \cdot \psi(x,y,z) = E\psi(x,y,z). \tag{4.7}$$

For each primal node p_{ij} we may write in DEC notation

$$(\mathscr{H}\bar{\psi}(x,y,z))|_{p_{i,j}=(x,y,z)} = -\frac{\hbar^2}{2m} \left(*_0^{-1} \mathrm{d}_0^T *_1 \mathrm{d}_0 \right) \bar{\psi}(p_{i,j}) + \bar{V}(p_{i,j})\bar{\psi}(p_{i,j}), \tag{4.8}$$

in which we defined $\bar{\psi}(p_{i,j}) = \bar{\psi}_{i,j}$, $\bar{V}(p_{i,j}) = \bar{V}_{i,j}$ so that Eq. (4.8) can be written as

$$\mathscr{H}\bar{\psi}_{i,j} = -\frac{\hbar^2}{2m} \left(*_0^{-1} \mathrm{d}_0^T *_1 \mathrm{d}_0 \right) \bar{\psi}_{i,j} + \bar{V}_{i,j}\bar{\psi}_{i,j}. \tag{4.9}$$

Now consider a primal edge $e_{i+s,j+k}$ such that $\partial e_{i+s,j+k} = \{p_{i,j}, p_{i+s,j+k}\}$, with $s,k = \{0,\pm 1\}$ (see Figure 8). The subscripts i and j refer to the position of primal nodes in the transverse and longitudinal directions, respectively. Then, for each $e_{i+s,j+k}$ we have

$$(d_0\bar{\psi})_{i,j} = \int_{e_{i+s,j+k}} d\bar{\psi} = \int_{\partial e_{i+s,i+k}} \bar{\psi} = (\bar{\psi}_{i+s,j+k} - \bar{\psi}_{i,j}), \tag{4.10}$$

consequently,

$$(*_1 d_0\bar{\psi})_{i,j} = \frac{|\star e_{i+s,j+k}|}{|e_{i+s,j+k}|}(\bar{\psi}_{i+s,j+k} - \bar{\psi}_{i,j}). \tag{4.11}$$

The r.h.s. of Eq. (4.10) then follows from (3.33). Taking the exterior derivative of the dual edge Eq. (4.11) we find

$$\left(d_0^T *_1 d_0\bar{\psi}\right)_{i,j} = \int_{(\star p_{i,j})} d*d\bar{\psi} = \int_{\partial(\star p_{i,j})} *d\bar{\psi} = \sum_{s=0,\pm1}\sum_{k=0,\pm1} \frac{|\star e_{i+s,j+k}|}{|e_{i+s,j+k}|}(\bar{\psi}_{i+s,j+k} - \bar{\psi}_{i,j}) \tag{4.12}$$

with $(s,k) \neq (0,0)$. Finally, applying $*_0^{-1}$ to Eq. (4.12) we get

$$\left(*_0^{-1} d_0^T *_1 d_0\bar{\psi}\right)_{i,j} = \sum_{s=0,\pm1}\sum_{k=0,\pm1} \frac{|\star e_{i+s,j+k}|}{|\star p_{i,j}||e_{i+s,j+k}|}(\bar{\psi}_{i+s,j+k} - \bar{\psi}_{i,j}) \qquad (s,k) \neq (0,0). \tag{4.13}$$

Therefore, the Schrödinger equation in DEC representation is given by

$$\begin{aligned} -t_{i,j+1}\bar{\psi}_{i,j+1} - t_{i,j-1}\bar{\psi}_{i,j-1} - t_{i+1,j}\bar{\psi}_{i+1,j} - t_{i-1,j}\bar{\psi}_{i-1,j} - t_{i+1,j+1}\bar{\psi}_{i+1,j+1} - t_{i-1,j-1}\bar{\psi}_{i-1,j-1} \\ + \left(\bar{V}_{i,j} + t_{i,j+1} + t_{i,j-1} + t_{i+1,j} + t_{i-1,j} + t_{i+1,j+1} + t_{i-1,j-1}\right)\bar{\psi}_{i,j} = E\bar{\psi}_{i,j}, \end{aligned} \tag{4.14}$$

where

$$t_{i+s,j+k} = \frac{\hbar^2}{2m}\frac{|\star e_{i+s,j+k}|}{|\star p_{i,j}||e_{i+s,j+k}|} \tag{4.15}$$

with $s,k \in \{0,\pm 1\}$ and $(s,k) \neq (0,0)$ are the hopping parameters for each slice in the transverse and longitudinal directions of the mesh.

The DEC version of the recursive technique for the Green's function is based on the slicing scheme, extensively used in flat systems (MACKINNON, 1985; USUKI et al., 1995; LAKE et al., 1997; LEWENKOPF; MUCCIOLO, 2013). In short, the slicing scheme consists in assuming that we can find the solution for each slice in the scattering region, and this slice is coupled to the preceding and succeeding slices by the hopping matrix terms of the discretized Schödinger equation. The system can be decomposed into N slices indexed by j containing M primal nodes as $i = 1,\ldots,M$, as shown in Figure 9. Slices with numbers 0 and $N+1$ represent the left and right leads, respectively. Here, we to adapting the procedures described in (FERRY; GOODNICK; BIRD, 2009) for our DEC-based Schödinger equation.

Figure 9 – Curved surface mesh (scattering region) used in the recursive Green's function approach. The color of the face of the triangles are mapped from the smallest (light color) to the largest deformation (dark color) in relation to the plane.

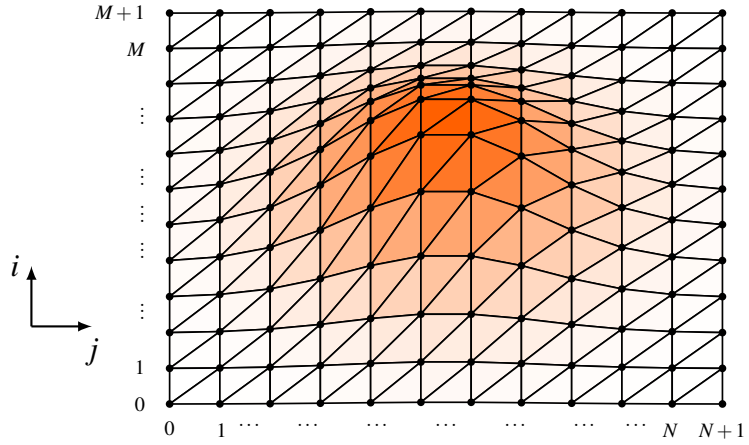

Source: (SILVA et al., 2019)

Rewriting Eq. (4.14) as a matrix equation we obtain

$$H_j\Psi_j - T_j\Psi_{j-1} - T_j^*\Psi_{j+1} - T_{j-1}\Psi_{j-1} - T_{j+1}\Psi_{j+1} = EI\Psi_j, \tag{4.16}$$

where

$$\Psi_j = \begin{bmatrix} \psi_{j,1} \\ \psi_{j,2} \\ \dots \\ \psi_{j,M} \end{bmatrix} \tag{4.17}$$

is vector wave function, at slice j, and

$$T_j = \begin{pmatrix} t_{j,1} & 0 & \dots & 0 \\ 0 & t_{j,2} & \dots & \dots \\ \dots & \dots & \dots & \dots \\ \dots & \dots & \dots & t_{j,M} \end{pmatrix}, \tag{4.18}$$

$$T_{j+1} = \begin{pmatrix} 0 & t_{j+1,1} & 0 & \dots & 0 \\ 0 & 0 & t_{j+1,2} & \dots & \dots \\ 0 & 0 & \dots & \dots & 0 \\ \dots & \dots & \dots & 0 & t_{j+1,M-1} \\ \dots & \dots & \dots & 0 & 0 \end{pmatrix}, \quad T_{j-1} = \begin{pmatrix} 0 & 0 & \dots & \dots & \dots \\ t_{j-1,1} & 0 & \dots & \dots & \dots \\ 0 & t_{j-1,2} & \dots & \dots & \dots \\ 0 & \dots & \dots & 0 & 0 \\ \dots & \dots & 0 & t_{j-1,M-1} & 0 \end{pmatrix}. \tag{4.19}$$

From Eq. (4.16) we conclude that the Hamiltonian of the system is a tridiagonal block of dimension $N \cdot M \times N \cdot M$ where the j^{th} block is the Hamiltonian of the j^{th} isolated slice given by

$$H_j = \begin{pmatrix} h_0(1,j) & t_{2,j} & \dots & 0 \\ t_{1,j} & h_0(2,j) & \dots & \dots \\ \dots & \dots & \dots & t_{M,j} \\ 0 & \dots & t_{M-1,j} & h_0(M,j) \end{pmatrix}, \tag{4.20}$$

with

$$h_0(i,j) = \sum_{s=0,\pm1} \sum_{k=0,\pm1} t_{i+s,j+k} + \bar{V}_{i,j} \quad (s,k) \neq (0,0). \tag{4.21}$$

The hopping matrices that make the coupling between the slices j and $j+1$ have dimension $M \times M$ and are given by

$$H_{j,j+1} = T_j + T_{j+1}, \qquad H_{j+1,j} = T_j + T_{j-1} \tag{4.22}$$

The recursive process is started by calculating the Green's function of the first slice

$$g^r_{1,1} = \left[E - H_1 - \Sigma^r_L\right]^{-1}. \tag{4.23}$$

Then, for each $j > 1$, we calculate the Green's functions for each slice through the following recurrence relations (LAKE et al., 1997):

$$g^r_{j+1,j+1} = \left[E - H_{j+1} - H_{j+1,j} g^r_{j,j} H_{j,j+1}\right]^{-1} \tag{4.24}$$

$$g^r_{j+1,1} = g^r_{j+1,j+1} H_{j+1,j} g^r_{j,1} \tag{4.25}$$

Finally, in the N^{th} slice, we obtain $G^r_{N,1}$ with

$$G^r_{N,N} = \left[E - H_N - H_{N,N-1} g^r_{N-1,N-1} H_{N-1,N} - \Sigma^r_R\right]^{-1} \tag{4.26}$$

$$G^r_{N,1} = G^r_{N,N} H_{N,N-1} g^r_{N-1,1} \tag{4.27}$$

The transmission at energy E is calculated using the formula (MEIR; WINGREEN, 1992):

$$T(E) = \mathrm{Tr}\left[\Gamma_L G^r_{N,1}(E) \Gamma_R G^a_{1,N}(E)\right], \tag{4.28}$$

where $G^a_{1,N} = \left[G^r_{N,1}\right]^\dagger$.

To summarize, the algorithm to obtain $G^r_{N,1}$ is:

Algorithm 1: DEC-based algorithm to calculate the retarded Green's functions

Data: Simplicial mesh $\mathscr{K}$
Result: $G^r_{N,1}$
compute Σ^r_L and Σ^r_R (Eq. (2.12);
compute $g^r_{1,1}$ (Eq. (4.23);
foreach *primal edge in the interior of* $\mathscr{K}$ **do**
  compute the volume according to sign convention Ref. (HIRANI; KALYANARAMAN; VANDERZEE, 2013)
end
foreach *dual edges and dual cells in the interior of* $\star\mathscr{K}$ **do**
  compute the volume according to sign convention Ref. (HIRANI; KALYANARAMAN; VANDERZEE, 2013)
end
for $j = 1$ **to** N **do**
  compute the matrices (4.18), (4.19) and (4.20);
  compute $g^r_{j+1,j+1}$ (Eq. (4.24);
  compute $g^r_{j+1,1}$ (Eq. (4.25);
  if *j is equal to N* **then**
    compute $G^r_{N,N}$ (Eq. (4.26));
    compute $G^r_{N,1}$ (Eq. (4.27));
  end
end

The computational cost of the our approach is in line with the typical RGF, i.e. it scales as $N \times M^3$, where N is the number of slices and M is the typical number of nodes in a given slice, see Figure 9. The recursive scheme presented here is particularly recommended for large systems in the presence of curvature. A schematic description of the whole procedure is shown in Figure 10. A performance comparison of the implementation of the models described in this section will be discussed in appendix A.

Figure 10 – Schematic depiction of the DEC-based procedure to calculate the retarded Green's functions. (color online)

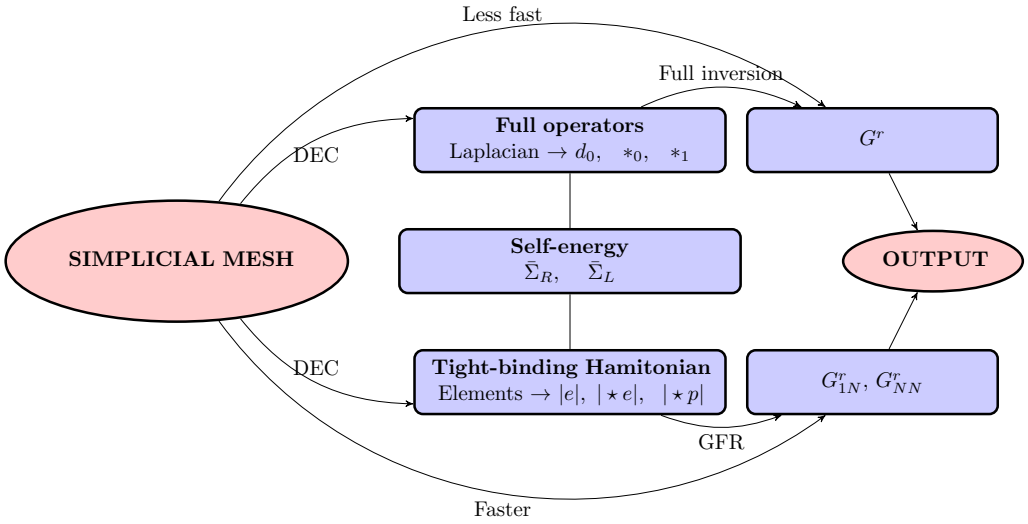

Source: (SILVA et al., 2019)

4.2 COMPARISON WITH FINITE DIFFERENCE IN FLAT SURFACE

Figure 11 – 2D structured-triangular mesh representing a flat surface with its primal e dual elements. The dual 2-cell $\star p_{i,j}$ is marked dashed lines and the dual 0-cells (circumcenters) marked with circles.

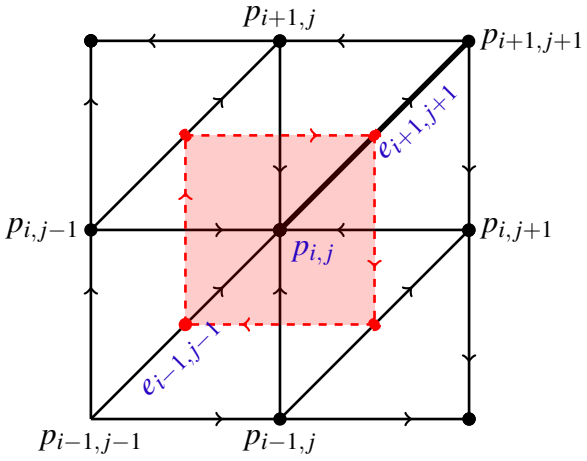

Source: (SILVA et al., 2019)

In order to compare the proposed DEC method with a known discretization method we consider the two-dimensional Schrödinger equation in flat space. The pairs of triangles that share the primal edges $e_{i+1,j+1}$ and $e_{i-1,j-1}$, have their circumcenters located at the same location (see Figure 11), then their respective dual edges have zero length. Defining triangular mesh with

lattice spacing a, the discrete Hodge star operators corresponding to nodes and edges are $*_0 = 1$ and $*_1 = a^2$, respectively. With due replacements in Eq. (4.15) we obtain

$$t_0 = t_{i,j+1} = t_{i,j-1} = t_{i+1,j} = t_{i-1,j} = \frac{\hbar^2}{2ma^2}, \tag{4.29}$$

$$\tag{4.30}$$

which leads to writing Eq. (4.14) as

$$t_0 \left(-\bar{\psi}_{i,j+1} - \bar{\psi}_{i,j-1} - \bar{\psi}_{i+1,j} - \bar{\psi}_{i-1,j}\right) + \left(4t_0 + V_{i,j}\right) \bar{\psi}_{i,j} = E\, \bar{\psi}_{i,j}. \tag{4.31}$$

Equation (4.31) coincides with the discrete representation of the Schrödinger equation in flat domains obtained with the FDM approach. Therefore, in addition to working with curved surfaces, our DEC-based discretization shares the advantages of FDM when submitted to structured-triangular mesh in flat space. In Appendix B, we present our DEC approach in quantum numerical simulations for both one-dimensional and two-dimensional domains (flat surface).

4.3 NUMERICAL RESULTS

As a simple application of our approach to an open system, we calculate the conductance of a curved sample. More specifically, the curved surface was generated by first generating a structured-triangular mesh (consisting of isosceles right triangles and vertical and horizontal spacing set to $a = 0.4nm$) on a $L \times W$ rectangular domain and then setting the z-coordinate value for the nodes as $z = \varphi(x,y) = A\exp(-(x^2+y^2)/b^2)$ (see Figure 7). The A parameter controls the maximum height of the Gaussian surface. Here, we have chosen values of b of the order 0.2 times of the system's width. The isolated semi-infinite leads Green's functions g^r_L and g^r_R (see Section 2.1) were approximated using the two-dimensional tight-binding Hamiltonian (FERRY; GOODNICK; BIRD, 2009). To emphasize the influence of curvature on the values of the conductance we considered the simplest case where the potential energy vanishes. Our DEC-based recursive technique is then used to obtain $G^r_{N,N}$ and $G^r_{N,1}$. Transmission coefficients were calculated using Eq. (4.28), which in turn were used to calculate the conductance via the Landauer formula.

Figure 12 – (a) Conductance versus energy of a curved system ($L = 24nm$ and $W = 12nm$) for increasing values of the curvature parametrized by the height A. (b) Cross-section of the Gaussian surface for four values of A.

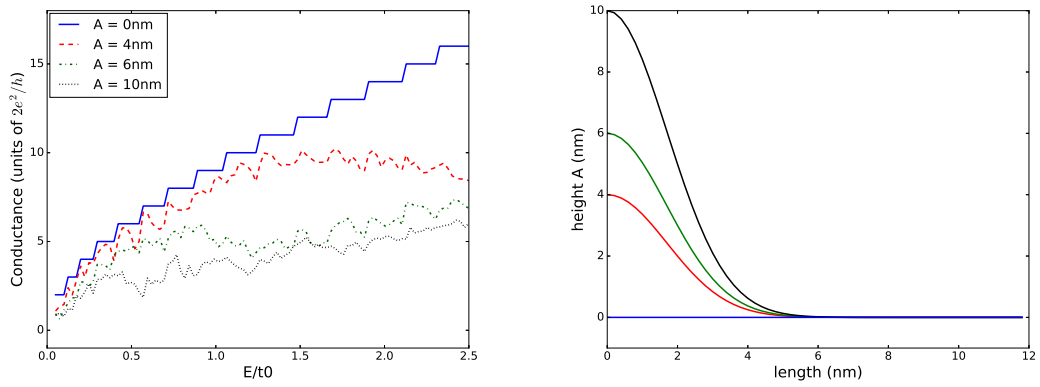

(a) (b)

Source: (SILVA et al., 2019)

Figure 13(a) shows the calculated conductance of curved systems with different levels of curvature, parametrized by the height A, as shown in Figure 12. Continuous line (relative to $A = 0$, i.e, for flat surface) can be related to the number of modes available for propagation. The qualitative change in the behavior of the conductance as a function of energy (for increasing curvatures) provides an interesting evidence of a possible crossover from an integrable regime, characterized by smooth conductance steps, towards a fluctuating Ericson-like energy dependence, typical of mixed or even chaotic systems (GUHR; MÜLLER-GROELING; WEIDENMÜLLER, 1998). A more detailed analysis of this curvature induced crossover in open systems is beyond the scope of this thesis and is left for a future work.

5 CONCLUSIONS

A discrete exterior calculus discretization of Schrödinger equation and of the associated Green's functions was developed. The discretizations were carried out through the discrete exterior calculus operators defined on a structured simplicial mesh and its circumcentric duality. Such an approach paved the way for the formulation of the DEC-based tight-binding Hamiltonian making it possible to explore the application of the recursive Green's function method in our model. Our approach results in an efficient method for the calculation of conductance on arbitrary surfaces with and without the presence of curvature. The ability to deal with curvature comprises a fundamental distinction between the DEC-based approach and others, such as FDM and FEM. It is worth remarking that as DEC is also applicable to unstructured simplicial meshes, we could have taken this approach to deal with curvature, but this choice would force the use of the full inversion model which, due to its complexity, makes quantum transport simulation in large systems impracticable. As an application to our DEC approach, we calculated the conductance of a curved quantum device coupled to two electron reservoirs. In this case, we found numerical evidences of a curvature induced integrable-chaotic crossover. Such evidence collaborates with investigations carried out in (SILVA et al., 2019), where, using the DEC formalism, the possible curvature-induced integrable-chaotic crossing is characterized through the statistical analysis of the corresponding spectra.

An additional merit of the presented methodology was to suppress the implement the discrete exterior derivative (d_0). As can be seen in Eq. (4.14), our tight-binding Hamiltonian depends only on the discrete Hodge star operators ($*_0$ and $*_1$) which in turn are restricted to the calculation of the length of primal and the calculation of the a flat or non-flat surface area, as described in Section 3.2.

We intend to extend the present work by proposing a DEC-based version of the covariant formulation of the Dirac equation in a curved space (LICHNEROWICZ, 1964; BIRRELL; BIRRELL; DAVIES, 1984) and use it to investigate the effects of curvature and topology on the electronic properties of a curved graphene sheet. Furthermore, we are developing a Python package with DEC-based algorithms to calculate transport properties in curved quantum systems for public use. There already exist several codes for solving the scattering problem (e.g., (KAZYMYRENKO; WAINTAL, 2008; GROTH et al., 2014)). However, so far, there is no package whose primary emphasis is to solve the scattering problem in complex geometries in the presence of curvature.

REFERENCES

ALOTTO FABIO FRESCHI, M. R. C. R. a. P. *The Cell Method for Electrical Engineering and Multiphysics Problems: An Introduction*. 1. ed. [S.l.]: Springer-Verlag Berlin Heidelberg, 2013. (Lecture Notes in Electrical Engineering 230).

ASSOUS, F.; DEGOND, P.; HEINTZE, E.; RAVIART, P.-A.; SEGRÉ, J. On a finite-element method for solving the three-dimensional maxwell equations. *Journal of Computational Physics*, Elsevier, v. 109, n. 2, p. 222–237, 1993.

ATANASOV, V.; DANDOLOFF, R. Curvature induced quantum potential on deformed surfaces. *Physics Letters A*, Elsevier, v. 371, n. 1-2, p. 118–123, 2007.

ATANASOV, V.; DANDOLOFF, R. Curvature-induced quantum behaviour on a helical nanotube. *Physics Letters A*, Elsevier, v. 372, n. 40, p. 6141–6144, 2008.

AUCHMANN, B.; KURZ, S. A geometrically defined discrete hodge operator on simplicial cells. *IEEE Transactions on Magnetics*, IEEE, v. 42, n. 4, p. 643–646, 2006.

BELL, N.; HIRANI, A. N. Pydec: software and algorithms for discretization of exterior calculus. *ACM Transactions on Mathematical Software (TOMS)*, ACM, v. 39, n. 1, p. 3, 2012.

BIRRELL, N. D.; BIRRELL, N. D.; DAVIES, P. *Quantum fields in curved space*. [S.l.]: Cambridge university press, 1984.

BOSSAVIT, A. *Computational electromagnetism: variational formulations, complementarity, edge elements*. [S.l.]: Academic Press, 1998.

CHEN, S. C.; CHEW, W. C. Electromagnetic theory with discrete exterior calculus. *Progress In Electromagnetics Research*, EMW Publishing, v. 159, p. 59–78, 2017.

CHEN, S. C.; CHEW, W. C. Numerical electromagnetic frequency domain analysis with discrete exterior calculus. *Journal of Computational Physics*, Elsevier, v. 350, p. 668–689, 2017.

CORTIJO, A.; VOZMEDIANO, M. A. Effects of topological defects and local curvature on the electronic properties of planar graphene. *Nuclear Physics B*, Elsevier, v. 763, n. 3, p. 293–308, 2007.

CORTIJO, A.; VOZMEDIANO, M. A. Electronic properties of curved graphene sheets. *EPL (Europhysics Letters)*, IOP Publishing, v. 77, n. 4, p. 47002, 2007.

COSTA, R. D. Quantum mechanics of a constrained particle. *Physical Review A*, APS, v. 23, n. 4, p. 1982, 1981.

DATTA, S. *Electronic transport in mesoscopic systems*. [S.l.]: Cambridge university press, 1997.

DATTA, S. *Quantum transport: atom to transistor*. [S.l.]: Cambridge University Press, 2005.

DESBRUN, M.; KANSO, E.; TONG, Y. Discrete differential forms for computational modeling. In: *Discrete differential geometry*. [S.l.]: Springer, 2008. p. 287–324.

DOLLFUS PHILIPPE; TRIOZON, F. *Simulation of transport in nanodevices*. 1. ed. [S.l.]: Wiley-ISTE, 2016. (Iste).

ELCOTT, S.; SCHRODER, P. Building your own dec at home. In: ACM. *ACM SIGGRAPH 2006 Courses*. [S.l.], 2006. p. 55–59.

ENCINOSA, M.; ETEMADI, B. Energy shifts resulting from surface curvature of quantum nanostructures. *Physical Review A*, APS, v. 58, n. 1, p. 77, 1998.

ENCINOSA, M.; MOTT, L. Curvature-induced toroidal bound states. *Physical Review A*, APS, v. 68, n. 1, p. 014102, 2003.

FERRETTI, E. *The cell method : a purely algebraic computational method in physics and engineering*. [S.l.]: Momentum Press, 2014.

FERRY, D.; GOODNICK, S. M. *Transport in nanostructures*. [S.l.]: Cambridge university press, 1997.

FERRY, D. K.; GOODNICK, S. M.; BIRD, J. *Transport in Nanostructures*. [S.l.]: Cambridge University Press, 2009.

GOES, F. de; DESBRUN, M.; MEYER, M.; DEROSE, T. Subdivision exterior calculus for geometry processing. *ACM Transactions on Graphics (TOG)*, ACM, v. 35, n. 4, p. 133, 2016.

GRADY, L. J.; POLIMENI, J. R. *Discrete calculus: Applied analysis on graphs for computational science*. [S.l.]: Springer Science & Business Media, 2010.

GROTH, C. W.; WIMMER, M.; AKHMEROV, A. R.; WAINTAL, X. Kwant: a software package for quantum transport. *New Journal of Physics*, IOP Publishing, v. 16, n. 6, p. 063065, 2014.

GUHR, T.; MÜLLER-GROELING, A.; WEIDENMÜLLER, H. A. Random-matrix theories in quantum physics: common concepts. *Physics Reports*, Elsevier, v. 299, n. 4-6, p. 189–425, 1998.

HAVU, P.; HAVU, V.; PUSKA, M. J.; NIEMINEN, R. M. Nonequilibrium electron transport in two-dimensional nanostructures modeled using green's functions and the finite-element method. *Physical Review B*, APS, v. 69, n. 11, p. 115325, 2004.

HIRANI, A. N. *Discrete exterior calculus*. Tese (Doutorado) — Citeseer, 2003.

HIRANI, A. N.; KALYANARAMAN, K.; VANDERZEE, E. B. Delaunay hodge star. *Computer-Aided Design*, Elsevier, v. 45, n. 2, p. 540–544, 2013.

JENSEN, H.; KOPPE, H. Quantum mechanics with constraints. *Annals of Physics*, Elsevier BV, v. 63, n. 2, p. 586–591, 1971.

JONES, E.; OLIPHANT, T.; PETERSON, P. Scipy: Open source scientific tools for python. *http://www. scipy. org/*, 2001.

JUAN, F. de; CORTIJO, A.; VOZMEDIANO, M. A. Charge inhomogeneities due to smooth ripples in graphene sheets. *Physical Review B*, APS, v. 76, n. 16, p. 165409, 2007.

KAZYMYRENKO, K.; WAINTAL, X. Knitting algorithm for calculating green functions in quantum systems. *Physical Review B*, APS, v. 77, n. 11, p. 115119, 2008.

KERNER, R.; NAUMIS, G. G.; GÓMEZ-ARIAS, W. A. Bending and flexural phonon scattering: Generalized dirac equation for an electron moving in curved graphene. *Physica B: Condensed Matter*, Elsevier, v. 407, n. 12, p. 2002–2008, 2012.

KOJIMA, K.; MITSUNAGA, K.; KYUMA, K. Calculation of two-dimensional quantum-confined structures using the finite element method. *Applied Physics Letters*, AIP, v. 55, n. 9, p. 882–884, 1989.

KURNIAWAN, O.; BAI, P.; LI, E. Ballistic calculation of nonequilibrium green's function in nanoscale devices using finite element method. *Journal of Physics D: Applied Physics*, IOP Publishing, v. 42, n. 10, p. 105109, 2009.

LAKE, R.; KLIMECK, G.; BOWEN, R. C.; JOVANOVIC, D. Single and multiband modeling of quantum electron transport through layered semiconductor devices. *Journal of Applied Physics*, AIP, v. 81, n. 12, p. 7845–7869, 1997.

LANDAUER, R. Conductance determined by transmission: probes and quantised constriction resistance. *Journal of Physics: Condensed Matter*, IOP Publishing, v. 1, n. 43, p. 8099, 1989.

LEWENKOPF, C. H.; MUCCIOLO, E. R. The recursive green's function method for graphene. *Journal of Computational Electronics*, Springer, v. 12, n. 2, p. 203–231, 2013.

LICHNEROWICZ, A. Champs spinoriels et propagateurs en relativité générale. *Bull. Soc. Math. France*, v. 92, n. 11, 1964.

MACKINNON, A. The calculation of transport properties and density of states of disordered solids. *Zeitschrift für Physik B Condensed Matter*, Springer, v. 59, n. 4, p. 385–390, 1985.

MANFREDO, P. *do Carmo. Differential geometry of curves and surfaces*. [S.l.]: Prentice Hall, 1976.

MARCHI, A.; REGGIANI, S.; RUDAN, M.; BERTONI, A. Coherent electron transport in bent cylindrical surfaces. *Physical Review B*, APS, v. 72, n. 3, p. 035403, 2005.

MEIR, Y.; WINGREEN, N. S. Landauer formula for the current through an interacting electron region. *Physical review letters*, APS, v. 68, n. 16, p. 2512, 1992.

MOHAMED, M. S.; HIRANI, A. N.; SAMTANEY, R. Comparison of discrete hodge star operators for surfaces. *Computer-Aided Design*, Elsevier, v. 78, p. 118–125, 2016.

MOHAMED, M. S.; HIRANI, A. N.; SAMTANEY, R. Discrete exterior calculus discretization of incompressible navier–stokes equations over surface simplicial meshes. *Journal of Computational Physics*, Elsevier, v. 312, p. 175–191, 2016.

MOHAMED, M. S.; HIRANI, A. N.; SAMTANEY, R. Numerical convergence of discrete exterior calculus on arbitrary surface meshes. *International Journal for Computational Methods in Engineering Science and Mechanics*, Taylor & Francis, v. 19, n. 3, p. 194–206, 2018.

MUNKRES, J. R. *Elements of algebraic topology*. [S.l.]: Addison-Wesley, Menlo Park, CA, 1984.

NESTLER, M.; NITSCHKE, I.; PRAETORIUS, S.; VOIGT, A. Orientational order on surfaces: The coupling of topology, geometry, and dynamics. *Journal of Nonlinear Science*, Springer, v. 28, n. 1, p. 147–191, 2018.

NITSCHKE, I.; REUTHER, S.; VOIGT, A. Discrete exterior calculus (dec) for the surface navier-stokes equation. In: *Transport Processes at Fluidic Interfaces*. [S.l.]: Springer, 2017. p. 177–197.

OLIPHANT, T. E. Python for scientific computing. *Computing in Science & Engineering*, IEEE, v. 9, n. 3, 2007.

PASK, J.; KLEIN, B.; STERNE, P.; FONG, C. Finite-element methods in electronic-structure theory. *Computer Physics Communications*, Elsevier, v. 135, n. 1, p. 1–34, 2001.

RABINA, J.; MONKOLA, S.; ROSSI, T. Efficient time integration of maxwell's equations with generalized finite differences. *SIAM Journal on Scientific Computing*, SIAM, v. 37, n. 6, p. B834–B854, 2015.

REN, Z.; VENUGOPAL, R.; GOASGUEN, S.; DATTA, S.; LUNDSTROM, M. S. nanomos 2.5: A two-dimensional simulator for quantum transport in double-gate mosfets. *IEEE Transactions on Electron Devices*, IEEE, v. 50, n. 9, p. 1914–1925, 2003.

RUFAT, D.; MASON, G.; MULLEN, P.; DESBRUN, M. The chain collocation method: A spectrally accurate calculus of forms. *Journal of Computational Physics*, Elsevier, v. 257, p. 1352–1372, 2014.

SANTOS, F.; FUMERON, S.; BERCHE, B.; MORAES, F. Geometric effects in the electronic transport of deformed nanotubes. *Nanotechnology*, IOP Publishing, v. 27, n. 13, p. 135302, 2016.

SILVA, L. C. da; BASTOS, C. C.; RIBEIRO, F. G. Quantum mechanics of a constrained particle and the problem of prescribed geometry-induced potential. *Annals of Physics*, Elsevier, v. 379, p. 13–33, 2017.

SILVA, L. D. da; BASTISTA, C. A.; GONZALEZ, I. R. R.; MACEDO, A. M.; OLIVEIRA, W. R. de; MELO, S. B. A discrete exterior calculus approach to quantum transport and quantum chaos on surface. *Journal of Computational and Theoretical Nanoscience*, 2019.

SPIVAK, M. *Calculus on Manifolds, vol. 1*. [S.l.]: WA Benjamin, New York, 1965.

STEGMANN, T.; SZPAK, N. Current flow paths in deformed graphene: from quantum transport to classical trajectories in curved space. *New Journal of Physics*, IOP Publishing, v. 18, n. 5, p. 053016, 2016.

STERN, A.; TONG, Y.; DESBRUN, M.; MARSDEN, J. E. Geometric computational electrodynamics with variational integrators and discrete differential forms. In: *Geometry, Mechanics, and Dynamics*. [S.l.]: Springer, 2015. p. 437–475.

SUZUURA, H.; ANDO, T. Phonons and electron-phonon scattering in carbon nanotubes. *Physical review B*, APS, v. 65, n. 23, p. 235412, 2002.

TAIRA, H.; SHIMA, H. Curvature effects on surface electron states in ballistic nanostructures. *Surface Science*, Elsevier, v. 601, n. 22, p. 5270–5275, 2007.

TAYLOR, C.; HOOD, P. A numerical solution of the navier-stokes equations using the finite element technique. *Computers & Fluids*, Elsevier, v. 1, n. 1, p. 73–100, 1973.

THOULESS, D.; KIRKPATRICK, S. Conductivity of the disordered linear chain. *Journal of Physics C: Solid State Physics*, IOP Publishing, v. 14, n. 3, p. 235, 1981.

TONTI, E. Why starting from differential equations for computational physics? *Journal of Computational Physics*, Elsevier, v. 257, p. 1260–1290, 2014.

TREVISAN, F.; KETTUNEN, L. Geometric interpretation of discrete approaches to solving magnetostatic problems. *IEEE transactions on magnetics*, IEEE, v. 40, n. 2, p. 361–365, 2004.

TSUCHIDA, E.; TSUKADA, M. Electronic-structure calculations based on the finite-element method. *Physical Review B*, APS, v. 52, n. 8, p. 5573, 1995.

TSUCHIDA, E.; TSUKADA, M. Adaptive finite-element method for electronic-structure calculations. *Physical Review B*, APS, v. 54, n. 11, p. 7602, 1996.

TUANN, S.-y.; OLSON, M. D. Numerical studies of the flow around a circular cylinder by a finite element method. *Computers & Fluids*, Elsevier, v. 6, n. 4, p. 219–240, 1978.

USUKI, T.; SAITO, M.; TAKATSU, M.; KIEHL, R.; YOKOYAMA, N. Numerical analysis of ballistic-electron transport in magnetic fields by using a quantum point contact and a quantum wire. *Physical Review B*, APS, v. 52, n. 11, p. 8244, 1995.

VOZMEDIANO, M. A.; JUAN, F. de; CORTIJO, A. Gauge fields and curvature in graphene. In: IOP PUBLISHING. *Journal of Physics: Conference Series*. [S.l.], 2008. v. 129, p. 012001.

WONG, M.-F.; PICON, O.; HANNA, V. F. A finite element method based on whitney forms to solve maxwell equations in the time domain. *IEEE Transactions on Magnetics*, IEEE, v. 31, n. 3, p. 1618–1621, 1995.

APPENDIX A – PERFORMANCE

We now show the performance comparison of the implementation of the recursive technique in Eqs. (4.26) and (4.27) and the full matrix inversion of Eq. (4.5), both corresponding to DEC applied to a standard quantum scattering problem: the calculation of conductance of a square curved system for a given fixed energy E. The system consists of $L \times L$ nodes that belong to a simplicial 3D mesh structured square (see Figure 9). The coupling of the system to the left and right semi-infinite leads of width L are attached. Measurements were performed on a computer with a 64-bit AMD A8-4500M processor and 8GiB of main memory running a GNU/Linux distribution with the SciPy (JONES; OLIPHANT; PETERSON, 2001) and NumPy (OLIPHANT, 2007) packages.

Figure 13 shows the dependence of the running time on L and compares the Green's function implementations based on DEC. The codes of both were written entirely in Python (using the NumPy and SciPy packages). One can see that for large system sizes, the recursive approach is up to a thousand times faster than the inversion method. As expected, our DEC-based approach has computational cost similar to FDM in calculating Green's functions as part of the solution to a scattering problem, i.e., $O(L^4)$.

Figure 13 – Time used to calculate the conductance of a curved square system of lateral length L. Circles: solutions using DEC full inversion implementation. Square: solutions using DEC recursive implementation. The lines show the theoretically expected sizing for large L: $O(L^6)$ for full inversion, $O(L^4)$ for the recursive technique.

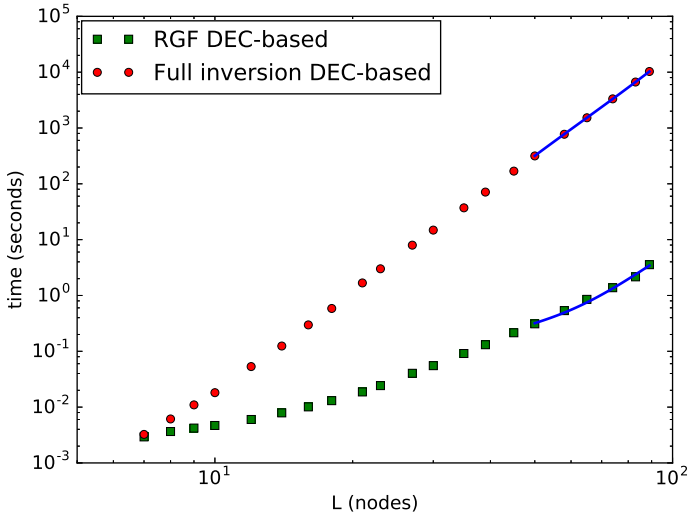

Source: (SILVA et al., 2019)

APPENDIX B – NUMERICAL SIMULATIONS

B.1 ONE-DIMENSIONAL QUANTUM WIRE

We compute the transmission probability through a one-dimensional quantum wire. The transmission probability is calculated using the Green's function approach. The problem of solving for the Green's functions numerically is formulated using the DEC (see Section 4.1.2). In Figure 15(a) shows the result of a numerical simulation using our DEC code compares with theoretical solution (FERRY; GOODNICK, 1997).

Figure 14 – The transmission coefficient calculated as a function of the electron energy.

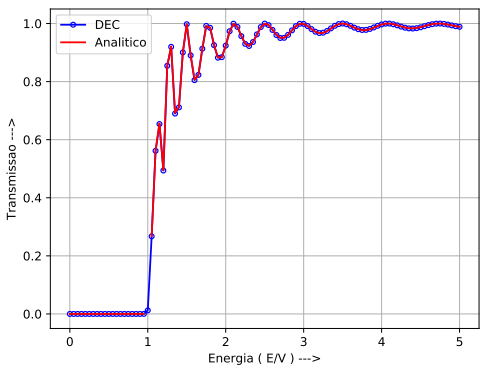

(a) Transmission probability versus energy for a simple symmetric barrier. Transmission versus energy for a simple symmetric barrier with length $W = 5$. In this calculation, the wire width is $L = 5$, and $V_0 = 10$. The solid line corresponds to theoretical solution and circles are calculated using the DEC code. The average distance between the DEC mesh nodes $a = 0.2$.

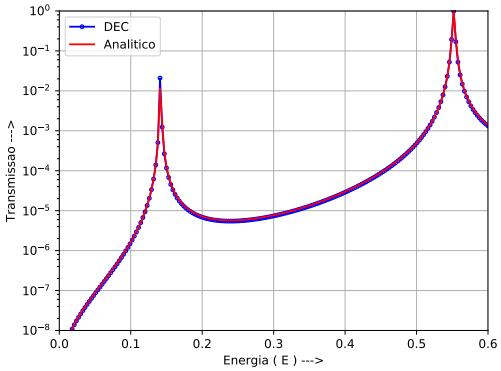

(b) Transmission probability versus energy for a double symmetric barrier with constant potential $V = 1.355$ and width of the $0.23L$. Here, the wire width is $L = 1.0$. The solid line corresponds to theoretical solution and circles are calculated using the DEC code. The average distance between the DEC mesh nodes $a = 0.2$.

Source: The author (2019)

B.2 TWO-DIMENSIONAL QUANTUM WIRE

We compute the transmission probability through a two-dimensional quantum wire (flat surface). The transmission probability is calculated using the Green's function approach. The problem of solving for the Green's functions numerically is formulated using the DEC (see Section 4.1.2). Figure 15 shows the results of a numerical simulations using our DEC code (Figure 16(b) compares with Kwant software (Figure 16(a)) (GROTH et al., 2014) (Python package for numerical calculations on tight-binding models).

Figure 15 – The transmission probability calculated as a function of the electron energy. The system is represented by a flat surface with length $L = 8nm$ and width $W = 4nm$. The distance between the DEC mesh nodes $a = 0.5nm$. The potential energy V at each vertex varies between $-t_0$ and t_0.

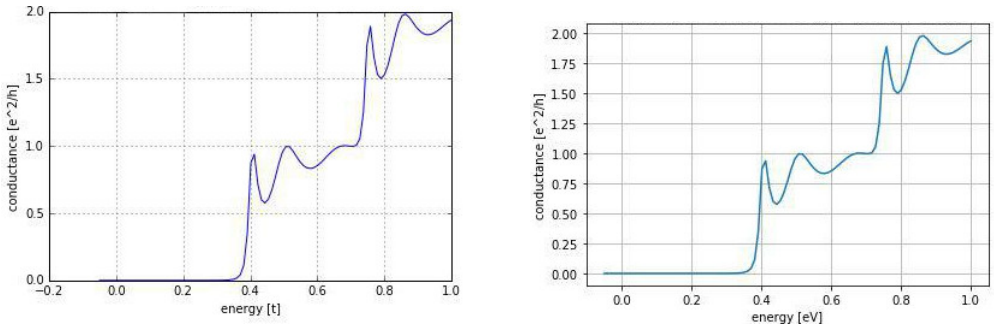

(a) Kwat 1.3. (b) DEC code.

Source: The author (2019)